AMERICAN UNIVERSITY OF BEIRUT

COUNTER-ROTATING DISKS AROUND BLACK HOLES

by

ADNAN IMAD NAHLAWI

A thesis
submitted in partial fulfillment of the requirements
for the degree of Master of Science
to the Department of Physics
of the Faculty of Arts and Sciences
at the American University of Beirut

Beirut, Lebanon
March 2013

AMERICAN UNIVERSITY OF BEIRUT

COUNTER-ROTATING DISKS AROUND BLACK HOLES

by

ADNAN IMAD NAHLAWI

Approved by:

Dr. Jihad Touma, Professor — Advisor
Physics

L Klushin

Dr. Leonid Klushin, Professor — Committee Member
Physics

M. El-Eid

Dr. Mounib El-Eid, Professor — Committee Member
Physics

On behalf of Dr. Seshadri Sridhar

Dr. Seshadri Sridhar, Professor — Committee Member
Physics

Date of thesis defense: March 22, 2013

AMERICAN UNIVERSITY OF BEIRUT

THESIS RELEASE FORM

I, Adnan Imad Nahlawi

☐ authorize the American University of Beirut to supply copies of my thesis to libraries or individuals upon request.

☐ do not authorize the American University of Beirut to supply copies of my thesis to libraries or individuals for a period of two years starting with the date of the thesis deposit.

_____

Signature

_____

Date

ACKNOWLEDGEMENTS

It is a great pleasure to acknowledge the support and the help of many figures without whom this thesis might not have been possible.

I would like to thank first and foremost my advisor Dr. Jihad Touma for the continuous support, encouragement and immense knowledge. His guidance helped me through challenging times of my research.

My deepest appreciation also goes to my thesis committee: Dr. Leonid Klushin, Dr. Mounib El-Eid and Dr. Seshadri Sridhar for their enriching comments and helpful discussions.

In addition, a big Thank you to my fellow graduates who made my life easier by providing me with a familial atmosphere.

I'm truly indebted and thankful to my parents: to my father Imad and my mother Zeina who never stopped boosting my morale, to my brother Mohammad and my sister Acile, my hope in this life, and to my sister Layan and my brother-in-law Sherief Oteafy; despite the distance, they have been and always will be very close.

My thanks also go to my uncle Mustafa Chebaro who is always there in the difficult times.

And last but not least, my fiancé Laiyan. I cannot find words to express my gratitude and appreciation to all what she did for me. The thesis would not happen to be possible without her being by my side supporting, encouraging and preventing me from giving up.

AN ABSTRACT OF THE THESIS OF

Adnan Imad Nahlawi for Master of Science
Major: Physics

Title: Counter-Rotating Disks Around Black Holes

The collective behavior of stars around a black hole provides great insights into the structure of galaxies. Thus, the focal point of this thesis is to study the dynamics of a cluster of stars within the radius of influence of a black hole in a galactic nucleus. Our approach to this nearly Keplerian system follows a semi-analytical treatment of the collisionless Boltzmann equation. Not interested in the fast orbital phase, we average over it and we focus our work on the study of the secular evolution of the resulting massive rings of constant semi-major axes. We further incorporate counter-rotation between stars and we divide our rings into two populations, prograde and retrograde, where different orbital semi-major axes are assigned to each population. Having the self-consistency of the problem with the absence of collisions, we represent the two populations of rings by two separate distribution functions (DFs), which satisfy two separate collionsless Boltzmann equations (CBEs) governed by two orbit-averaged Hamiltonians (ring Hamiltonians). To describe populations of rings of small eccentricities, we expand the ring Hamiltonians to fourth order in the eccentricities and we build upon Jeans' theorem to construct statistical distribution functions representing the eccentric rings. When the dispersion in eccentricity is relatively small, these distribution functions are completely described by their centroids. The dynamics of centroids are shown to be equivalent to a two-degree-of-freedom Hamiltonian system. This system turned out to be integrable due to the presence of two conserved quantities, the Hamiltonina itself, and another quantity corresponding to the total angular momentum of the two populations. Using the conservation of the angular momentum, we reduce the system into a one-degree-of-freedom system that can be studied through phase space analysis. The linear as well as the nonlinear dynamics of the system are studied, where a criterion of linear instability is derived for initially circular discs. In addition, the phase space structure and bifurcations are explored as a function of parameters like the angular momentum, the mass and the semi-major axis ratio of the stellar populations.

CONTENTS

ILLUSTRATIONS

CHAPTER I

INTRODUCTION

One of the challenging and inspiring aspects of Astrophysics is the study of stellar objects (e.g. galaxies, star clusters, etc) so large and so far to the extent that we cannot experiment on them. Actually, all what we can measure of these objects are billion-year late electromagnetic waves reflecting an extremely old image of them. Our only hope to better understand these objects is through the astrophysical tools of analytical modeling or computational numerical simulations.

In analytical modeling, theorists try to construct mathematical models that match a set of observational constraints and satisfy physical laws at the same time. To model a star cluster for example, a representative library of allowed orbits in the given potential is determined (Schwarzschild's orbit superposition technique) [1]. One tries then to find the combination of orbits that best fits the observed photometry and kinematics of the stellar object. The application of such techniques usually allow for a wide range of models. However, the problem remains to choose the "real" model between all possible models. We assume that the stability and the instability of the system can be used to discriminate between possibilities [2]. It may reject a model or help in choosing between several alternate or conflicting models.

Galactic nucleus is one of the exiting stellar objects studied nowadays. Galactic nucleus is a compact region at the center of a galaxy (within 40 pc of the Galactic center). It is very bright, its luminosity is much higher than the normal one. It is believed to contain high density of stars (the average distance between neighboring stars in the Galactic center is only 0.005 pc) orbiting around a massive black hole ($\sim$ 4 million the mass of the sun).

The dynamics of a star in a galactic nucleus involves physical processes of com-

plicated nature which could be simplified by several approximations especially in a small region around the Black hole. For instance, if we consider a region around a black hole where the mass of the enclosed stellar system is small enough compared to the mass of the black hole, we can consider each star as moving under a dominant gravitational attraction of the black hole plus a relatively small, but not negligible, self-gravity of the stellar system (i.e. all the other stars). In this case, we can regard the dynamics in this region of the galactic nucleus as a perturbation of the Kepler problem (where the only existing force is the force due to the central body) [2], and each star may be thought of as moving on a Keplerian ellipse that slowly presses and deforms in time. We call such systems "nearly Keplerian" systems.

As an example of a nearly Keplerian system, we take the center of a Milky-way-like galaxy which contains a black hole of mass $\sim 4 \times 10^6\ M_\odot$. Based on the stellar density in this compact region, one can show that the enclosed stellar mass within a radius of 1 pc is $\sim 1.4 \times 10^6\ M_\odot$ which is less than the half of the mass of the black hole. So the stellar system in the Galactic center can be considered as a nearly Keplerian system for $r \lesssim 1$ pc. Moreover, ignoring relativistic effects, our discussion becomes applicable only to distances beyond several Schwarzschild radii from the black hole.

Nearly Keplerian stellar systems may be subject to secular stabilities as well as instabilities due to the slow precession of counter-rotating stellar populations around the black hole [2]. The secular evolution of such systems shows a rich dynamics leading to various equilibrium configurations corresponding to uniformly precessing eccentric orbits of aligned or anti-aligned periapses. These equilibria (stable or unstable) could explain many astronomical observations like the lopsidedness of some galactic nuclei. In fact, Hubble Space Telescope shows that the nucleus of $M31$ (Andromeda galaxy) contains two separated components of different brightness [3].

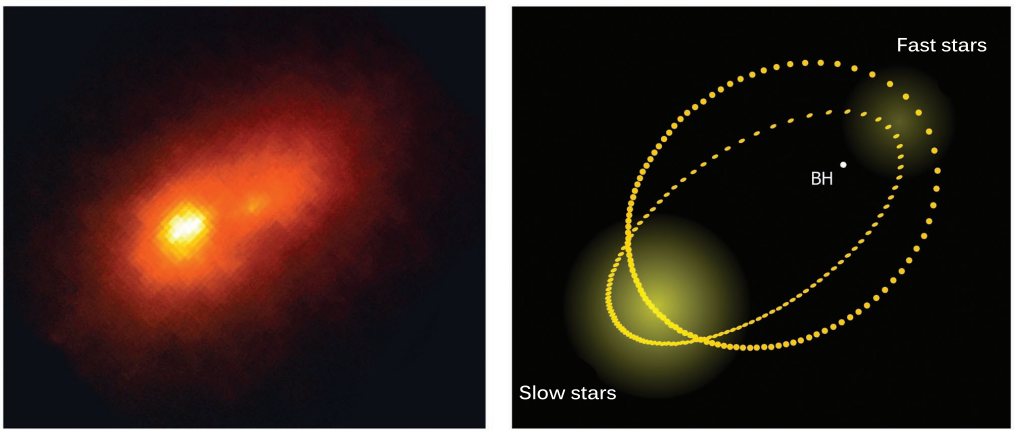

Figure 1: Andromeda Galaxy, $M31$

The brighter component is offset from the center of the galaxy, whereas the dimmer component falls at the center of the galaxy. The currently favored model that explains the main observed features assumes that the nucleus is an eccentric stellar disk, composed of stars traveling on nearly Keplerian orbits of aligned periapses around a black hole [4]. The model suggests that the periapses of the orbits are aligned. The brighter component is the region of the nuclear disk close to apoapsis and has high surface brightness because the stars slow down near apoapsis, while the dimmer component is the region of the nuclear disk close to periapsis and has lower surface brightness because the velocity of stars near the periapsis is high so they weakly contribute to the surface brightness [5].

In this work, we develop a semi-analytic treatment of the self-consistent problem of cluster of stars around a massive black hole, and explore the associated dynamics. The theory provides conditions for linear instability of counter-rotating clusters, as well as the location and nature of equilibria as a function of parameters like the total angular momentum of the stellar system, the mass and the semi major axis ratio of the counter-rotating populations. The stars in the cluster are assumed to move on nearly Keplerian orbits around the black hole due to the dominance of the black hole within its radius of influence. As we are not interested in the fast orbital phase, we average over it and we focus our work on the study of the secular evolution (the slow precession and deforma-

tion) of the resulting massive rings (Gaussian rings). Having the self-consistency and the absence of collisions in the problem, we represent the two populations of rings by two distribution functions (DFs), which satisfy collionsless Boltzmann equations (CBEs) governed by orbit-averaged Hamiltonians (ring Hamiltonians). Restricting our problem to populations of rings of small eccentricities, we then expand the ring Hamiltonians to fourth order in the eccentricities. Using Jeans' theorem, we construct our time-dependent DFs. The resulting DFs turn out to be such that their isocontours are ellipses centered at moving origins. Those moving origins, refer to as the centroids, satisfy four equations. The four centroid equations are shown to be equivalent to an underlying Hamiltonian corresponding to a two-degree-of-freedom system. This system turn out to be integrable due to the presence of two conserved quantities, the Hamiltonina itself, and another quantity corresponding to the total angular momentum of the two populations which allow us to reduce the system into a one-degree-of-freedom system that can be studied using the phase space analysis.

The thesis is organized as follows. Chapter 2 provides a simple preview where we start with studying the problem of one star around a black hole then the problem of two stars around a black hole. These two problems lead us to the more general problem of a cluster of stars around a black hole. We present general strategies and approximations to solve such N-body problems and we introduced the collisionless systems. Chapter 3 contains a formulation of the problem of counter-rotating clusters of stars around a black hole. In order to study the corresponding dynamics we model the system by specifying the phase space, then constructing the distribution functions representing the system and finally formulating the Hamiltonians governing the collisionless Boltzmann equations. Chapter 4 contains a complete study of the dynamics of DF centroids, starting from the four equations introduced in chapter 3, then deriving the underlying Hamiltonian. The chapter also provides a linear as well as nonlinear study of the centroid dynamics leading to instability and phase space analysis. Finally, a summary and conclusions will be offered in chapter 5.

CHAPTER II

MOTIVATION

Before studying the dynamics of counter-rotating clusters of stars around a black hole (which is an N-body problem with N very large), we would like to start with the simpler problems of one star around a black hole and two stars around a black hole.

A. One star around a black hole

This is a two-body problem (Kepler problem), where we have two bodies that interact with each other through their mutual gravitational attraction. For simplicity, we treat the black hole and the star as if they are mass points, without any size. In this case they will not collide, unless they happen to hit each other head-on. However, for random initial conditions, the chance of such a collision is negligible. The two-body problem can be considered as two independent one-body problems, a problem that involves solving for the motion of one particle in an external static potential. Hence, the 2-body problem can be solved analytically.

We now start solving our two-body problem by reducing it to two independent one-body problems. Let $\mathbf{x}_1$ and $\mathbf{x}_2$ be the positions of the star and the black hole respectively, and m_1 and m_2 be their masses. Applying Newton's second law to the two masses gives

$$\mathbf{F}_{12} = m_1 \ddot{\mathbf{x}}_1 \tag{1}$$

$$\mathbf{F}_{21} = m_2 \ddot{\mathbf{x}}_2 \tag{2}$$

where $\mathbf{F}_{12}$ is the gravitational force done on mass 1 (the star) by mass 2 (the black hole), and $\mathbf{F}_{21}$ is the gravitational force done on mass 2 (the black hole) by mass 1 (the star).

Adding equations 1 and 2 results in an equation describing the motion of the center of mass:

$$m_1\ddot{\mathbf{x}}_1 + m_2\ddot{\mathbf{x}}_2 = \mathbf{F}_{12} + \mathbf{F}_{21} = 0 \tag{3}$$

$$\Rightarrow (m_1 + m_2)\ddot{\mathbf{R}} = 0 \tag{4}$$

where we have used the fact that $\mathbf{F}_{12} = -\mathbf{F}_{21}$ and where

$$\ddot{\mathbf{R}} = \frac{m_1\ddot{\mathbf{x}}_1 + m_2\ddot{\mathbf{x}}_2}{m_1 + m_2}$$

$\mathbf{R}$ is the position of the center of mass of the system (star-black hole). The resulting equations:

$$\ddot{\mathbf{R}} = 0 \tag{5}$$

$$\Rightarrow \dot{\mathbf{R}} = \text{const} \tag{6}$$

show that the center of mass of the system moves with constant velocity. By contrast, subtracting equation 2 from equation 1 results in an equation describing how the position vector of the star relative to the black hole changes with time:

$$\ddot{\mathbf{x}}_1 - \ddot{\mathbf{x}}_2 = \frac{\mathbf{F}_{12}}{m_1} - \frac{\mathbf{F}_{21}}{m_2} \tag{7}$$

$$\Rightarrow \ddot{\mathbf{r}} = (\frac{1}{m_1} + \frac{1}{m_2})\mathbf{F}_{12} \tag{8}$$

where we have again used Newton's third law $\mathbf{F}_{12} = -\mathbf{F}_{21}$ and where $\mathbf{r} = \mathbf{x}_1 - \mathbf{x}_2$ is the relative position vector from the black hole to the star. The force $\mathbf{F}_{12}$ between the star and the black hole is the gravitational force which is only a function of their separation r and it is given by:

$$\mathbf{F}_{12} = -\frac{Gm_1m_2}{r^2}\hat{\mathbf{r}} \tag{9}$$

where $\hat{\mathbf{r}} = \frac{\mathbf{r}}{r}$. Equation (8) can therefore be written:

$$\mu \ddot{\mathbf{r}} = -\frac{G\mu(m_1+m_2)}{r^2}\hat{\mathbf{r}} \tag{10}$$

where $\mu = \frac{m_1 m_2}{m_1+m_2}$ is the reduced mass. From this equation, we see that the star moves around the black hole as if it was a point particle of mass μ moving under the gravitational force of a stationary body of mass (m_1+m_2) located at the position of the black hole. Since this gravitational force is always pointing towards the black hole, we know from spherical symmetry that the angular momentum vector $\mathbf{L}$ of the fictitious particle is conserved in magnitude and direction. Conservation of the direction of $\mathbf{L}$ implies that the particle's motion lies in a plane perpendicular to the constant vector $\mathbf{L}$. Thus, without loss of generality, we can take the inclination angle $\theta = \frac{\pi}{2}$. The remaining generalized coordinates can be then taken to be the polar coordinates (r, ϕ). The Lagrangian of this problem is then given by:

$$\mathscr{L} = \frac{1}{2}\mu(\dot{r}^2 + r^2\dot{\phi}^2) + \frac{Gm_1m_2}{r} \tag{11}$$

Using the Lagrange equation for the coordinate r, and the conservation of the magnitude L of angular momentum, we obtain:

$$\mu\ddot{r} = \frac{L^2}{\mu r^3} - \frac{Gm_1m_2}{r^2} \tag{12}$$

where $L = \mu r^2\dot{\phi}$. Switching from time to angle variables and substitute $r = \frac{1}{u}$. This gives:

$$\frac{d^2u}{d\phi^2} + u = \frac{G(m_1+m_2)\mu^2}{L^2} \tag{13}$$

which can be solved to give conic section solutions, including the elliptical orbit as a special case. In this problem, we are mainly interested in the elliptical orbit solution

given in the polar coordinates by

$$r(\phi) = \frac{a(1-e^2)}{1+e\cos(\phi-\phi_0)} \tag{14}$$

where e is the eccentricity and a the semi-major axis. In this case, the star orbits the black hole on an ellipse, with the black hole being located at one of the foci of that ellipse.

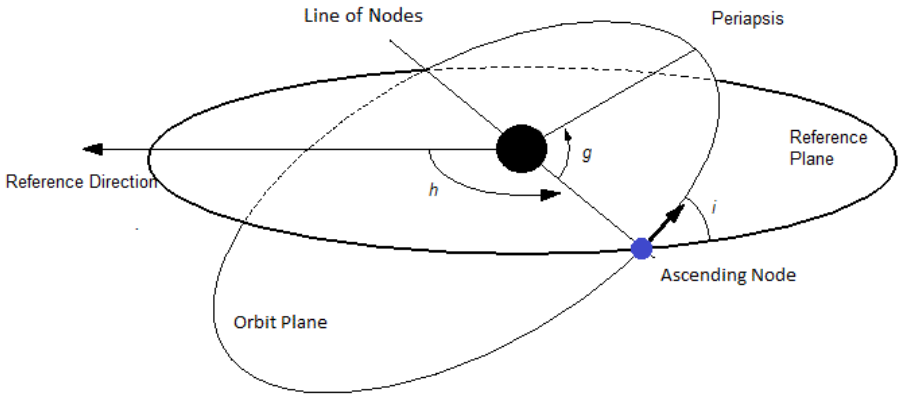

Figure 2: Orbital elements

The elliptical orbit and the position of the star describing it can be defined in the space by six quantities called the orbital elements [6]. The first element is the longitude h of the ascending node, which is the angle from a reference direction to the ascending node. The second element is the inclination i, which is the angle between the orbital plane and a reference plane. The third element is the longitude g of periapsis, which defines the orientation of the ellipse within the orbital plane. The fourth element is the eccentricity e which is the measure of the elliptical departure from a circle. The fifth element is the semi-major axis a, which is the half of the sum of the periapsis and apoapsis distances. The sixth element is the mean anomaly ω, which defines the position of the orbiting star along the ellipse at a specific time.

Note that for $m_1 << m_2$ (as it is the case for the black hole compared to the star) we have

$$\mathbf{R} = \frac{m_1\mathbf{x}_1 + m_2\mathbf{x}_2}{m_1 + m_2} \simeq \mathbf{x}_2 \tag{15}$$

Therefore, the black hole which is approximately located at the center of mass is considered as either at rest or moving with constant velocity in a straight line.

Although determining $\mathbf{R}(t)$ and $\mathbf{r}(t)$ is enough for understanding the behavior of the system (star-black hole), the original trajectories may be obtained explicitly

$$\mathbf{x}_1(t) = \mathbf{R}(t) + \frac{m_2}{m_1 + m_2}\mathbf{r}(t) \tag{16}$$

$$\mathbf{x}_2(t) = \mathbf{R}(t) - \frac{m_1}{m_1 + m_2}\mathbf{r}(t) \tag{17}$$

The total energy of the system (star-black hole) is conserved, not the energy of each body. It is true that the energy of the individual particle is conserved in the one-body problem and for the 'fictitious' particle of mass μ in the two-body problem. But it is not true of each of the separate bodies in the two-body problem. Same thing for the angular momentum.

The 2-body problem (Kepler problem) can be used to provide a first order approximation to the motions of several stars around a black hole where the stars are considered independent. It can also serve as a starting point for the generation of analytical solutions for the motions of several interacting stars around a black hole, through perturbation theory [6].

B. Two stars around a black hole

This is a three-body problem where three bodies interact with each other through their mutual gravitational attraction. Whereas the two-body problem was completely

solved analytically, the three-body problem, apart from some special cases, is not solvable in the sense that analytical expressions describing the behavior of the bodies for all times cannot be obtained [7]. In general, the three-body problem results in chaotic motion with no obvious sign of a repetitious path. Hence, we have to do numerical calculations for special configurations of initial conditions or some approximations using perturbation theory for some convenient applications. Due to the large mass of the black hole relative to the two stars, it is obvious that the mutual attraction between the two stars is so much smaller than the black hole's attraction upon them. Hence, we can regard the dynamics in this case as a perturbation of the two-body problem (Kepler problem). We call this kind of systems "nearly Keplerian systems". As a first order approximation, we can consider the system as two independent two-body problems without taking into account the force between the stars. With this approximation, the two stars will orbit the black hole on two independent fixed ellipses with the black hole located at a common focus of these ellipses. (fig. 3)

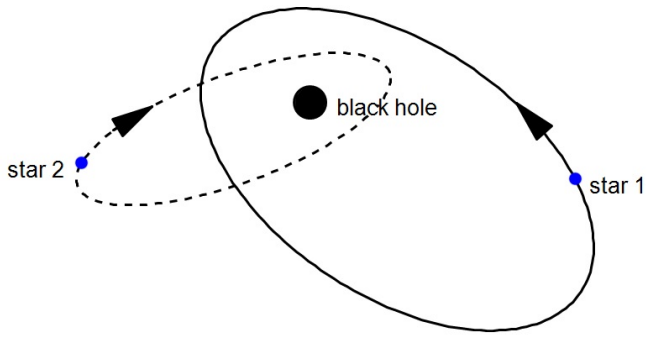

Figure 3: First approximation of the two-star-black hole problem: the two stars orbit the black hole on two independent fixed ellipses.

On the other hand and as a higher order approximation, the system is considered as a two-body problem (the black hole and one star) plus a perturbative force (due to the second star). With this approximation, the two stars orbit the black hole on two slowly varying ellipses with the black hole located at a common focus of these ellipses (fig. 14). The ellipses may change orientation as well as shape. Note that the two stars may be

rotating in the same direction or counter-rotating, depending on the initial conditions and the dynamical behavior of the system.

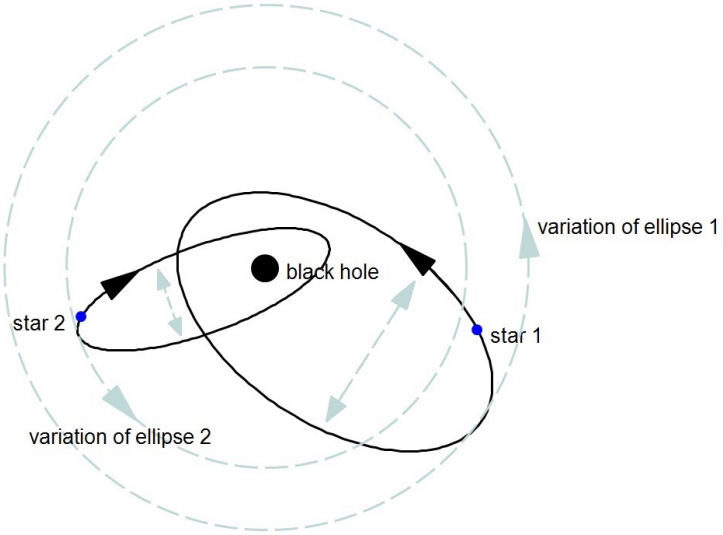

Figure 4: Second approximation of the two-star-black hole problem: the two stars orbit the black hole on two slowly varying ellipses (in shape and orientation).

1. Orbital averaging

Under this approximation, one can differ between two different timescales; the fast orbital timescale at which a star orbits the BH and the slow secular time scale at which the stellar orbits evolve. When the timescale under consideration is much larger than the orbital timescale and with certain assumptions concerning the secular time scale, we can average over the orbital phase and focus our study on the secular evolution of the resulting massive rings. Therefore, instead of dealing with a star that moves on a nearly Keplerian orbit, we deal with a massive ring focused at the black hole. The massive ring is thought of as an ellipse populated by many stars which are distributed inversely proportional to their orbital velocity. For more information concerning the averaging process, see the next chapter.

C. Cluster of stars around a black hole in a galactic nucleus

This is an N-body problem where N bodies interact with each other through their mutual gravitational attraction. As mentioned before, for $N > 2$ almost all problems become non-integrable and we must resort to computational techniques or approximations and perturbation theory [6]. This N-body problem is similar to the three-body problem in the sense that it can be approximated in the same way but with perturbative force corresponding to all the other stars instead of one star.

1. Galaxies as collisionless systems

As a first approximation, we discuss the subject of collisionless systems. We might think that stars, as they move inside a galaxy, will experience strong encounters with other stars as well as weak encounters that change the dynamics. The truth, however, is different. Strong star-star encounters are extremely rare in galaxies, and the effects of weak encounters are so slight that it takes an extremely long time for the dynamics of galaxies to change substantially [8].

Starting with the strong encounters, we consider two stars of mass m that approach to a distance r. We can consider this encounter as strong if the potential energy of the two stars during this encounter is larger than the typical kinetic energy of a star in a galaxy [8]

$$\frac{Gm^2}{r} > \frac{1}{2}mv^2 \implies r < \frac{2Gm}{v^2}$$

where v is the typical velocity of a star in the galaxy. Hence, a strong encounter occurs if two stars approach to within a distance $r_s \equiv \frac{2Gm}{v^2}$.

As an example, consider a Milky-way-like galaxy where the typical velocity of a star is $v \approx 200$ km/s and its mass is roughly the mass of the sun, $m \approx 2 \times 10^{30}$ kg, using these values, we can estimate the strong encounter distance as $r_s \simeq 7 \times 10^9$ m. This is very small relative to the typical separation a between stars in a galaxy; $a \simeq \times 10^{16}$ m. Therefore,

strong encounters are very rare in galaxies. In practice, we can ignore their effect on the dynamics of stars.

On the other hand, we can infer from the previous discussion that a weak encounter occurs if two stars approach to a minimum distance $r_s \equiv \frac{2Gm}{v^2}$. Weak encounters in general cause only a small perturbation to the motions of stars in a stellar system, but they are so much more numerous than strong encounters and may become more important than strong encounters in a collective manner. We shall now determine the cumulative effect of large number of weak encounters on the velocity of a star crossing a galaxy.

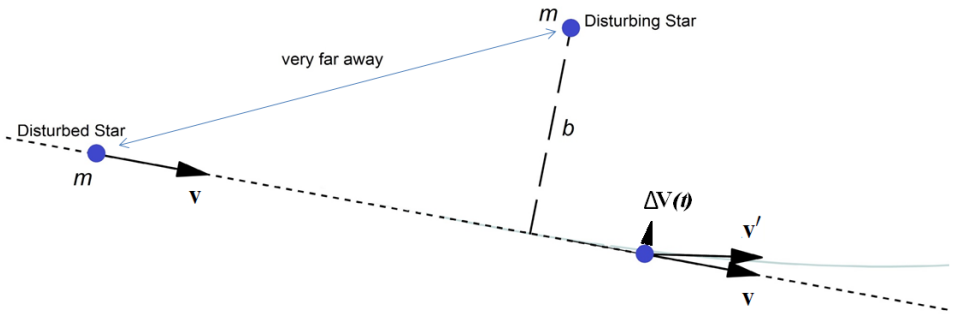

Figure 5: A star of mass m approaching a perturbing star of the same mass at an impact parameter b.

Consider a star of mass m approaching a perturbing star of the same mass m at an impact parameter b. Assume that the impact parameter b is larger than r_s. Hence, the encounter between these two stars is a weak encounter. Because the encounter is weak, the approaching star is considered to be moving on a straight line where the tangential velocity is constant and the change in velocity in the perpendicular direction is very small but not negligible.

Let's determine now the velocity change of a crossing star due to one weak encounter. At any time t when the separation between the two stars is r, the component of the gravitational force perpendicular to the direction of motion will be

$$F_\perp = \frac{Gm^2}{r^2}\sin\theta \tag{18}$$

Taking $r \simeq \sqrt{b^2+v^2t^2}$ where $t=0$ at the point of closest approach and using $\sin\theta = \frac{b}{r} \simeq \frac{b}{\sqrt{b^2+v^2t^2}}$, we get

$$F_\perp = \frac{Gm^2 b}{(b^2+v^2t^2)^{\frac{3}{2}}} \tag{19}$$

Applying Newton's second law, perpendicular to the direction of motion we obtain

$$a_\perp = \frac{Gmb}{(b^2+v^2t^2)^{\frac{3}{2}}} \tag{20}$$

$$\Rightarrow \frac{dv_\perp}{dt} = \frac{Gmb}{(b^2+v^2t^2)^{\frac{3}{2}}} \;\Rightarrow\; dv_\perp = \frac{Gmb}{(b^2+v^2t^2)^{\frac{3}{2}}}dt \tag{21}$$

where $v_\perp$ is the component at time t of the velocity perpendicular to the initial direction of motion. To get the total change in velocity due to one encounter, we integrate from time $t=-\infty$ to $+\infty$,

$$|\Delta\mathbf{v}| = \Delta v_\perp = \int_0^{v_{\perp f}} dv_\perp = \int_{-\infty}^{+\infty} \frac{Gmb}{(b^2+v^2t^2)^{\frac{3}{2}}}dt \tag{22}$$

After solving this integral

$$|\Delta\mathbf{v}| = \frac{2Gm}{bv} \tag{23}$$

As a star moves through space, it will experience a number of perturbations caused by all the weak encounters. The resulting deflections in velocity $\Delta\mathbf{v}$ are random in direction, so they add up to zero. However, the effect when we add them in quadrature is significant and this is what we should consider

$$\Delta v^2 = |\Delta\mathbf{v}|^2 = \left(\frac{2Gm}{bv}\right)^2 \tag{24}$$

Consider now the effect of all weak encounters occurring in a time period t. Consider a spherical system of size R and N stars with a star crossing it with velocity v. The number

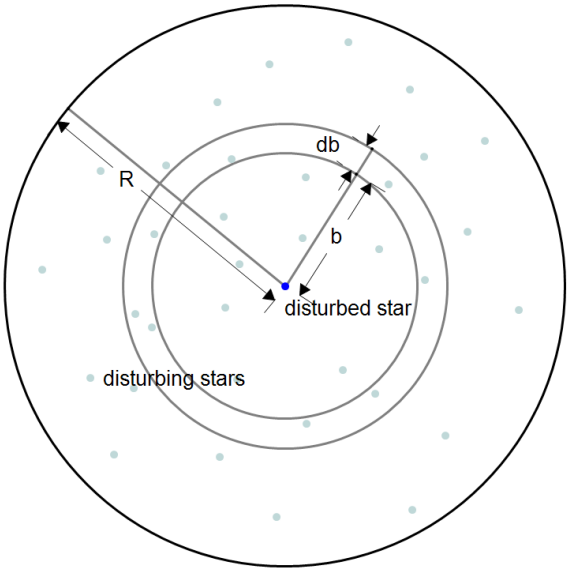

Figure 6: Cross section of a spherical system of size R crossed by a star at the center, where b is the impact parameter.

of stars encountered with impact parameters between b and $b+db$ in time t is

$$\mathrm{d}n = \frac{N}{\frac{4}{3}\pi R^3}\, 2\pi b\, \mathrm{d}b\, vt = \frac{3Nb\, vt\, \mathrm{d}b}{2R^3} \tag{25}$$

The total squared deflection caused by all the encounters of impact parameters between b and $b+\mathrm{d}b$ will be

$$\Delta v^2 = \left(\frac{2Gm}{bv}\right)^2 \left(\frac{3Nb\, vt\, \mathrm{d}b}{2R^3}\right) \tag{26}$$

Integrating over b, the total squared deflection in a time t due to all encounters of impact parameters between $b_{\min}$ and $b_{\max}$ is

$$\begin{aligned} \Delta v^2 &= \int_{b_{\min}}^{b_{\max}} \left(\frac{2Gm}{bv}\right)^2 \left(\frac{3Nb\, vt\, \mathrm{d}b}{2R^3}\right) \\ \Rightarrow \Delta v^2 &= 6\left(\frac{Gm}{v}\right)^2 \left(\frac{Nvt}{R^3}\right) \ln\left(\frac{b_{\max}}{b_{\min}}\right) \end{aligned}$$

The relaxation time T_{relax} is defined as the time taken for the effect of weak encounters to

become significant i.e. for $\Delta v^2 = v^2$. Replacing Δv^2 by v^2 in the previous equation we get

$$v^2 = 6\left(\frac{Gm}{v}\right)^2 \left(\frac{NvT_{\text{relax}}}{R^3}\right) \ln\left(\frac{b_{\max}}{b_{\min}}\right)$$

$$\Rightarrow\ T_{\text{relax}} = \frac{1}{6N\ln\left(\frac{b_{\max}}{b_{\min}}\right)} \frac{(Rv)^3}{(Gm)^2} \tag{27}$$

Taking $b_{\max} = R$ and $b_{\min} = r_s$, we get

$$T_{\text{relax}} = \frac{1}{6N\ln\left(\frac{R}{r_s}\right)} \frac{(Rv)^3}{(Gm)^2} \tag{28}$$

Using this equation, we can estimate the relaxation time for a system of stars, such as a galaxy.

As an example, consider again a Milky-way like galaxy where the typical velocity of a star is $v = 200$ km/s, its mass is $m = 2\times10^{30}$ kg, $N = 10^{10}$, $R = 3\times10^{20}$ m, and $r_s = 7\times10^9$ m. Using these values, we get the relaxation time as $T_{\text{relax}} \simeq 10^{25}$ s $\simeq 10^{17}$ yr. This relaxation time is 10^7 times the typical age of a galaxy which is $\sim 10^{10}$ yr.

So, in addition to the strong encounters, weak encounters are of no significance for galaxies. Therefore, galaxies are considered as collisionless systems where collisions encounters between stars are ignored.

At this point, it is useful to review the three relevant timescales encountered so far, the orbital timescale, the secular timescale and the relaxation timescale. The orbital timescale is the timescale on which the star orbits the black hole. It can be determined through:

$$v_{\text{orb}} = \frac{2\pi r}{t_{\text{orb}}} \quad \Rightarrow \quad t_{\text{orb}} = \frac{2\pi r}{v_{\text{orb}}}$$

where r is the average orbital radius. v_{orb} can be recovered from the centripetal force relation $F_{\text{grav}} = \frac{v^2}{r}$

$$\Rightarrow \quad \frac{v^2}{r} = \frac{GM_\bullet}{r^2} \quad \Rightarrow \quad v = \sqrt{\frac{GM_\bullet}{r}}$$

$$\Rightarrow \quad t_{\rm orb} = \frac{2\pi r^{\frac{3}{2}}}{GM_\bullet^{\frac{1}{2}}}$$

The secular timescale is the timescale on which orbits precess and evolve. It's related to the orbital time through the fact that

$$\frac{t_{\rm sec}}{t_{\rm orb}} = \frac{M_\bullet}{M_{\rm stars}} \quad \Rightarrow \quad t_{\rm sec} = \frac{M_\bullet}{M_{\rm stars}}\, t_{\rm orb}$$

The relaxation time scale is the time taken for the collisions and encounters in the system to become significant. For nearly Keplerian systems these three timescales are well separated:

$$t_{\rm orb} << t_{\rm sec} << t_{\rm relax}$$

For instance, in the Galactic center and very close to the black hole, $t_{\rm orb} \sim 10^4$ yrs, $t_{\rm sec} \sim 10^5$ and $t_{\rm relax} \sim 10^{10}$ yrs.

CHAPTER III

MODELING AND FORMULATION

Consider a collisionless cluster of stars surrounding a black hole in a galactic nucleus. In order to study the dynamical behavior of the stars, we need first to model the system by specifying the phase space in which the system can be described, then constructing the distribution functions representing the system and finally formulating the Hamiltonians governing the dynamics of the system. Before starting, it's useful to define here the sphere of influence of a black hole.

A. Sphere of influence

The sphere of influence is a region around a black hole in which the gravitational potential of the BH dominates the gravitational potential of the surrounding stars. The radius of this sphere is called the radius of influence r_h. One way to determine the radius of influence is through:

$$M_{\text{stars}}(r \leqslant r_h) \ll M_\bullet$$

where $M_\bullet$ is the mass of the black hole and M_{stars} is the mass of the surrounding stellar system. As an example, consider the nearest normal galactic nuclei; the nucleus of our galaxy and the nucleus of $M31$. In the case of our galaxy there is evidence for back hole of mass $\sim 4 \times 10^6\ M_\odot$ [2]. Given the stellar density around the black hole, we find the radius of influence $r_h \approx 1$ pc. Within the sphere of influence, the mass of the stellar system is $\sim 1.4 \times 10^6\ M_\odot < \frac{1}{2} M_\bullet$ which is small enough for the black hole to dominate the dynamics. On the other hand, $M31$ has a black hole of mass $\sim 1 \times 10^8\ M_\odot$ [9]. For a stellar density $\sim 2500\ M_\odot\ \text{pc}^{-3}$, $r_h \sim 16$ pc.

We can also determine the radius of influence of a black hole through the velocity dispersion of the surrounding stellar system. If the velocity dispersion in the stellar system is σ, we can say that the black hole has a strong influence on the stellar dynamics if the radius of influence is given by

$$r_h = \frac{GM_\bullet}{\sigma^2}$$

For $M31$ and $\sigma \sim 166$ km/s, we obtain again $r_h \sim 16$ pc.

By definition, the mass of the stellar system is much smaller than the mass of the black hole within the radius of influence. In this case, we consider each star as moving under a dominant gravitational attraction of the black hole plus a relatively small, self-gravity of the stellar system (i.e. all the other stars). Therefore, we can regard the dynamics in this region as a perturbation of the two-body problem (Kepler problem). We call such systems "nearly Keplerian systems".

B. Phase space

Each star in our system is represented by a moving point in the 6-dimensional phase space, $(\mathbf{r}, \mathbf{v})$, where $\mathbf{r}$ is its position with respect to the black hole and $\mathbf{v}$ is its velocity. For nearly Keplerian systems, it is useful to use the Delaunay variables as the phase space variables. The Delaunay variables are action-angle variables for the Kepler problem and they are more or less equivalent to the orbital elements defined in the previous chapter [10]

- ω is the mean anomaly, it is related to the position angle θ of the star on the orbit, $\omega = n\,(t - T)$, where $n = \frac{2\pi}{\tau}$ and T is time at periapsis.
- g is the argument of periapsis measured from the ascending node.
- h is the argument of node measured from the reference direction to the ascending node.

- I is the conjugate momentum to the mean anomaly, it is related to the semi-major axis a, $I = \sqrt{GM_\bullet a}$, where $M_\bullet$ is the mass of the black hole.

- L is the magnitude of angular momentum vector, it is related to the eccentricity e, $L = \sqrt{GM_\bullet a(1-e^2)}$.

- L_z is the z-projection of the angular momentum vector, where the z-axis is taken to be perpendicular to the reference plane, it is related to the inclination i through $L_z = \sqrt{GM_\bullet a(1-e^2)}\cos i$.

The self gravity of the system is defined as the gravitational attraction upon a star due to all the other stars. In the absence of the self gravity, the motion of any star would be purely Keplerian. The star would move on a fixed elliptical orbit where g, h, I, L, and L_z are all constant and ω advances steadily at a specific orbital frequency. The Delaunay variables are, by definition, the action-angle variables in this case, which implies that the Hamiltonian of the system is $H = H(I;L;Lz)$, where ω, g and h are all cyclic. However in the presence of self gravity, the Delaunay variables, g, h, I, L, and L_z, are not constant any more. They are slowly varying in time due to the small self gravity within the radius of influence of BH. In this case, stars move on nearly Keplerian orbits, elliptical orbits that are slowly evolving in time (changing orientation and shape).

Hence, one can differ between two timescales; the fast orbital timescale at which ω advances and the slow secular timescale at which g, h, L, L_z and I evolve. When the timescale, weŠre interested in, is much larger than the orbital timescale, one may average over the orbital phase and integrate over the corresponding variable ω. Integrating over ω, the orbit-averaged Hamiltonian becomes $H = H(I;L;Lz;g;h;t)$ where ω is the only cyclic variable now. Since H is independent of ω, the conjugate momentum I is a constant of motion and by definition of I the semi-major axes of orbits are constant in time. The averaging process predicts that the semi-major axis has no secular evolution. This leads to a third different timescale of the problem at which the semi-major axis advances. For consistency, this third time scale should be much slower than the secular one so that we

can neglect any change in the semi-major axis on the faster secular time scale. Therefore, Averaging process is valid for any time scale that is much slower than the orbital one and at the same time much faster than the semi-major axis one.

Hence our phase space can be reduced now to a 4-dimensional phase space, (L, L_z, g, h) without ω and with I as a parameter defining different populations of stars in the phase space. Moreover, if the star is restricted to a planar motion, we won't have the phase-space variables L_z and h any more (h and g no longer have clear independent meanings). Hence our phase space becomes 2-dimensional, (g, L) where

- g is the argument of periapsis.
- L is the algebraic magnitude of angular momentum vector, it is related to the eccentricity e and the direction of rotation (prograde or retrograde), $L = \pm\sqrt{GM_\bullet a(1-e^2)}$.

It's more convenient to normalize L and deal with $l = \pm\sqrt{1-e^2}$ such that $-1 < l < 1$ instead of $L = \pm\sqrt{GM_\bullet a(1-e^2)}$ [11]. Hence the phase space becomes (g, l), where

- g is the argument of periapsis.
- l is the normalized algebraic magnitude of angular momentum vector, it is related to the eccentricity e and the direction of rotation (prograde or retrograde), $l = \pm\sqrt{(1-e^2)}$.

The corresponding Hamiltonian of the system becomes $H_{\text{new}} = \frac{H_{\text{old}}}{\sqrt{GM_\bullet a}}$. Each point in the phase space (g, l) represents now a ring with the following properties:

1. All rings are focused at the black hole.
2. All rings are restricted to a plane.
3. We assume for simplicity that every ring has a constant direction of rotation; prograde or retrograde (i.e. a ring cannot switch membership from the prograde to the retrograde population).

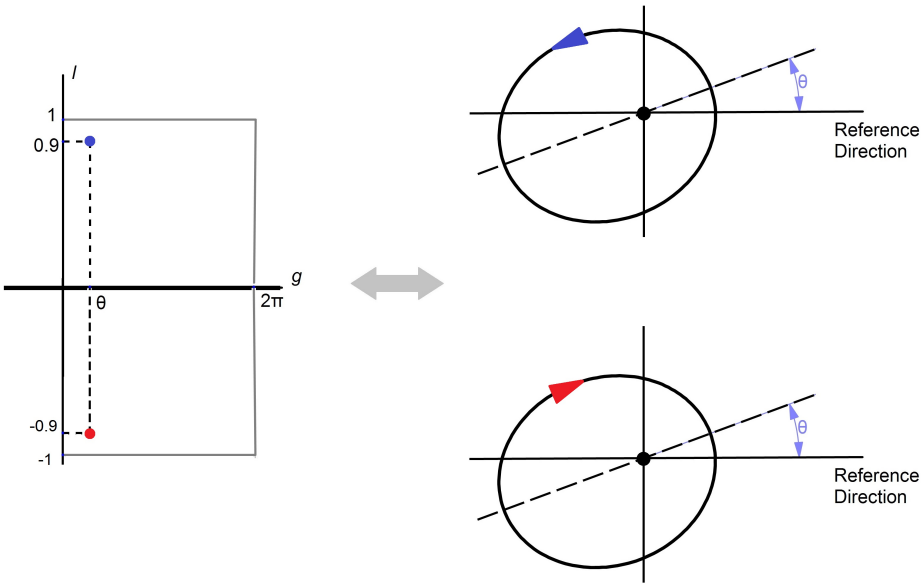

Figure 7: (l,g) phase space and the real space for two counter-rotating stars.

4. We assume for simplicity that all the prograde rings have the same constant semi-major axis a_+ and all the retrograde rings have the same constant semi-major axis a_-.

5. Every ring has a variable orientation g and variable eccentricity e.

To summarize, the system is composed of two populations of elliptical rings evolving (i.e. precessing and deforming) in a plan around the black hole. The first population is prograde and has semi-major axis a_+ and the second population is retrograde and has semi-major axis a_-.

C. Distribution Function Concept

To describe the dynamics of a large number of rings in the phase space, it's more convenient to represent the rings using a continuous distribution function $f(l,g,t)$ instead of describing it ring by ring [11]. This is due mainly to two reasons:

1. It's not practical numerically to follow the dynamics of each ring.

2. The Hamiltonian governing any ring depends on the dynamics of all the other rings (due to ring-ring interactions). Thus, we represent all the rings by one distribution function f and take the Hamiltonian of any ring as a function of f (note that the distribution function f is self-consistently dependent on the Hamiltonian).

The distribution function f, as defined here, is the mass density of rings in the 2-dimensional phase space (i.e. the mass of rings with orientation between g and $g+\mathrm{d}g$ and with angular momentum between l and $l+\mathrm{d}l$ is $f(l,g,t)\ \mathrm{d}l\mathrm{d}g$). The total mass of the rings is given by the integration over the whole phase space, $M=\int f(l,g,t)\ \mathrm{d}l\mathrm{d}g$.

To derive an equation that governs the distribution functions of a collisionless system in the phase space, we start by the assumption that the number of stars is conserved in a galactic nucleus. This means ignoring star formation and the death of stars. This assumption results in a continuity equation of rings in the phase space, which relates the rate of change of the distribution function with time to the rates of change with position and velocity.

$$\frac{\partial f}{\partial t}+\frac{\partial}{\partial \mathbf{x}}(f\dot{\mathbf{x}})+\frac{\partial}{\partial \mathbf{v}}(f\dot{\mathbf{v}})=0 \tag{29}$$

Using the product rule, we get

$$\frac{\partial f}{\partial t}+\dot{\mathbf{x}}.\frac{\partial f}{\partial \mathbf{x}}+f\frac{\partial \dot{\mathbf{x}}}{\partial \mathbf{x}}+\dot{\mathbf{v}}.\frac{\partial f}{\partial \mathbf{v}}+f\frac{\partial \dot{\mathbf{v}}}{\partial \mathbf{v}}=0 \tag{30}$$

It is possible, in the case of collisionless systems, to derive an equation from the continuity equation that more explicitly states the relation between the distribution function f, position $\mathbf{x}$, velocity $\mathbf{v}$ and time t [8]. In fact, each point in the phase space is moving under a Hamiltonian dynamics which gives $\dot{\mathbf{x}}$ and $\dot{\mathbf{v}}$ in terms of H

$$\dot{\mathbf{x}}=\frac{1}{m}\frac{\partial H}{\partial \mathbf{v}} \qquad\qquad \dot{\mathbf{v}}=-\frac{1}{m}\frac{\partial H}{\partial \mathbf{x}}$$

$$\Rightarrow \quad \frac{\partial \dot{\mathbf{x}}}{\partial \mathbf{x}}=\frac{1}{m}\frac{\partial}{\partial \mathbf{x}}\frac{\partial H}{\partial \mathbf{v}} \qquad \frac{\partial \dot{\mathbf{v}}}{\partial \mathbf{v}}=-\frac{1}{m}\frac{\partial}{\partial \mathbf{v}}\frac{\partial H}{\partial \mathbf{x}}$$

$$\Rightarrow \quad f\frac{\partial \dot{\mathbf{x}}}{\partial \mathbf{x}} = -f\frac{\partial \dot{\mathbf{v}}}{\partial \mathbf{v}}$$

Therefore, the third and the fifth terms cancel out in the equation and we're left with the collisionless Boltzmann equation (CBE)

$$\frac{\partial f}{\partial t} + \mathbf{v}.\frac{\partial f}{\partial \mathbf{x}} - \nabla\Phi.\frac{\partial f}{\partial \mathbf{v}} = 0 \tag{31}$$

where we used $\dot{\mathbf{x}} = \mathbf{v}$ and $\dot{\mathbf{v}} = -\nabla\Phi$, Φ is the gravitational potential of the system. The collisionless Boltzmann equation is the equation that governs the collisionless evolution of stars in a galactic nucleus. It tells us that $df/dt = 0$. This means that the probability density in phase space, does not change with time for a test particle. The CBE is given in terms of the gravitational potential Φ. At the same time, the potential Φ of the system is given self-consistently (by Poisson's equation) in terms of the DF f. In other words, the collisionless Boltzmann equation and the Poisson's equation, together constitute a system of two equations with two unknowns (f and Φ):

$$\frac{\partial f}{\partial t} + \mathbf{v}.\frac{\partial f}{\partial \mathbf{x}} - \nabla\Phi.\frac{\partial f}{\partial \mathbf{v}} = 0$$

$$\nabla\Phi(\mathbf{x}) = 4\pi G\,\rho(\mathbf{x})$$

where $\rho(\mathbf{x})$ is the mass density at point $\mathbf{x}$, it's related to the distribution function through $\rho = \int f\ \mathrm{d}\mathbf{v}$.

It is more convenient to take separate distribution functions $f^+(l,g,t)$ and $f^-(l,g,t)$ for the prograde and the retrograde populations [11], such that:

$\int f^+ \mathrm{d}l\mathrm{d}g = M^+$, mass of all the prograde rings

$\int f^- \mathrm{d}l\mathrm{d}g = M^-$, mass of all the retrograde rings

and satisfying the collisionless Boltzmann equations:

$$\begin{aligned}\frac{\partial f^+}{\partial t}+[f^+,H^+] &= 0\\ \frac{\partial f^-}{\partial t}+[f^-,H^-] &= 0\end{aligned}$$

D. Ring Hamiltonian

In addition to the attraction of the black hole, each ring interacts gravitationally with every other ring without collisions causing precession and deformation. The secular evolution (precession and deformation) of any ring is governed by the following Hamiltonian:

Prograde ring

$$\begin{aligned}H^+(l,g,t) &= -\int \mathrm{d}l'\mathrm{d}g'\ f^+(l',g',t)\ \sqrt{\frac{G}{M_\bullet a_+}}\Psi(a_+,l,g;a_+,l',g')\\ &\quad -\int \mathrm{d}l'\mathrm{d}g'\ f^-(l',g',t)\ \sqrt{\frac{G}{M_\bullet a_+}}\Psi(a_+,l,g;a_-,l',g')\end{aligned}$$

Retrograde ring

$$\begin{aligned}H^-(l,g,t) &= -\int \mathrm{d}l'\mathrm{d}g'\ f^+(l',g',t)\ \sqrt{\frac{G}{M_\bullet a_-}}\Psi(a_-,l,g;a_+,l',g')\\ &\quad -\int \mathrm{d}l'\mathrm{d}g'\ f^-(l',g',t)\ \sqrt{\frac{G}{M_\bullet a_-}}\Psi(a_-,l,g;a_-,l',g')\end{aligned}$$

where:

- $\Psi(a_+,l,g;a_+,l',g')$ is the interaction function between two prograde rings.
- $\Psi(a_+,l,g;a_-,l',g')$ is the interaction function between an unprimed prograde ring and a primed retrograde ring.

- $\Psi(a_-, l, g; a_+, l', g')$ is the interaction function between an unprimed retrograde ring and a primed prograde ring.
- $\Psi(a_-, l, g; a_-, l', g')$ is the interaction function between two retrograde rings.

1. Interaction Function Expansion

In general the interaction function Ψ can be expanded in terms of $\boldsymbol{e}$ and $\boldsymbol{e'}$. It is given to the fourth order [11] by:

$$\begin{aligned}\Psi(a,e,g;a',e',g') &= \frac{\rho}{2\max(a,a')}\Big(c_1e^2 + c_2\boldsymbol{e}.\boldsymbol{e'} + c_3e'^2 + c_4e^4 + c_5e^2(\boldsymbol{e}.\boldsymbol{e'}) \\ &\quad + c_6e^2e'^2 + c_7(\boldsymbol{e}.\boldsymbol{e'})^2 + c_8(\boldsymbol{e}.\boldsymbol{e'})e'^2 + c_9e'^4\Big)\end{aligned}$$

$$\text{where} \qquad \rho = \frac{\min(a,a')}{\max(a,a')} \qquad \boldsymbol{e} = (e\cos g, e\sin g) \qquad \boldsymbol{e'} = (e'\cos g', e'\sin g')$$

Without loss of generality, let's assume that $a_+ > a_-$, Ψs are then given by [11]:

$$\begin{aligned}\Psi(a_+,e,g;a_+,e',g') &= \left(\frac{1}{2a_+}\right)\Big(c_{20}^{0\,++}e^2 + c_{11}^{1\,++}\boldsymbol{e}.\boldsymbol{e'} + c_{40}^{0\,++}e^4 + c_{31}^{1\,++}e^2(\boldsymbol{e}.\boldsymbol{e'}) \\ &\quad + (c_{22}^{0\,++} - c_{22}^{2\,++})e^2e'^2 + 2c_{22}^{2\,++}(\boldsymbol{e}.\boldsymbol{e'})^2 + c_{13}^{1\,++}(\boldsymbol{e}.\boldsymbol{e'})e'^2\Big)\end{aligned}$$

$$\begin{aligned}\Psi(a_+,e,g;a_-,e',g') &= \left(\frac{a_-}{2a_+^{\,2}}\right)\Big(c_{20}^{0\,+-}e^2 + c_{11}^{1\,+-}\boldsymbol{e}.\boldsymbol{e'} + c_{40}^{0\,+-}e^4 + c_{31}^{1\,+-}e^2(\boldsymbol{e}.\boldsymbol{e'}) \\ &\quad + (c_{22}^{0\,+-} - c_{22}^{2\,+-})e^2e'^2 + 2c_{22}^{2\,+-}(\boldsymbol{e}.\boldsymbol{e'})^2 + c_{13}^{1\,+-}(\boldsymbol{e}.\boldsymbol{e'})e'^2\Big)\end{aligned}$$

$$\begin{aligned}\Psi(a_-,e,g;a_+,e',g') &= \left(\frac{a_-}{2a_+^{\,2}}\right)\Big(c_{02}^{0\,+-}e^2 + c_{11}^{1\,+-}\boldsymbol{e}.\boldsymbol{e'} + c_{04}^{0\,+-}e^4 + c_{13}^{1\,+-}e^2(\boldsymbol{e}.\boldsymbol{e'}) \\ &\quad + (c_{22}^{0\,+-} - c_{22}^{2\,+-})e^2e'^2 + 2c_{22}^{2\,+-}(\boldsymbol{e}.\boldsymbol{e'})^2 + c_{31}^{1\,+-}(\boldsymbol{e}.\boldsymbol{e'})e'^2\Big)\end{aligned}$$

$$\begin{aligned}\Psi(a_-,e,g;a_-,e',g') &= \left(\frac{1}{2a_-}\right)\Big(c_{02}^{0\,--}e^2 + c_{11}^{1\,--}\boldsymbol{e}.\boldsymbol{e'} + c_{04}^{0\,--}e^4 + c_{13}^{1\,--}e^2(\boldsymbol{e}.\boldsymbol{e'}) \\ &\quad + (c_{22}^{0\,--} - c_{22}^{2\,--})e^2e'^2 + 2c_{22}^{2\,--}(\boldsymbol{e}.\boldsymbol{e'})^2 + c_{31}^{1\,--}(\boldsymbol{e}.\boldsymbol{e'})e'^2\Big)\end{aligned}$$

Hence we can write:

$$\begin{aligned}
\sqrt{\frac{G}{M_\bullet a_+}}\Psi(+,+') &= \alpha_{++}e^2+\beta_{++}\boldsymbol{e}.\boldsymbol{e'}+\chi_{++}e^4+\nu_{++}e^2(\boldsymbol{e}.\boldsymbol{e'}) \\
&\quad +\gamma_{++}e^2e'^2+\lambda_{++}(\boldsymbol{e}.\boldsymbol{e'})^2+\kappa_{++}(\boldsymbol{e}.\boldsymbol{e'})e'^2 \\
\sqrt{\frac{G}{M_\bullet a_+}}\Psi(+,-') &= \sqrt{\frac{a_-}{a_+}}\Big(\alpha_{cp}e^2+\beta_c\boldsymbol{e}.\boldsymbol{e'}+\chi_{cp}e^4+\kappa_{cp}e^2(\boldsymbol{e}.\boldsymbol{e'}) \\
&\quad +\gamma_c e^2e'^2+\lambda_c(\boldsymbol{e}.\boldsymbol{e'})^2+\kappa_{cm}(\boldsymbol{e}.\boldsymbol{e'})e'^2\Big) \\
\sqrt{\frac{G}{M_\bullet a_-}}\Psi(-,+') &= \alpha_{cm}e^2+\beta_c\boldsymbol{e}.\boldsymbol{e'}+\chi_{cm}e^4+\kappa_{cm}e^2(\boldsymbol{e}.\boldsymbol{e'}) \\
&\quad +\gamma_c e^2e'^2+\lambda_c(\boldsymbol{e}.\boldsymbol{e'})^2+\kappa_{cp}(\boldsymbol{e}.\boldsymbol{e'})e'^2 \\
\sqrt{\frac{G}{M_\bullet a_-}}\Psi(-,-') &= \alpha_{--}e^2+\beta_{--}\boldsymbol{e}.\boldsymbol{e'}+\chi_{--}e^4+\nu_{--}e^2(\boldsymbol{e}.\boldsymbol{e'}) \\
&\quad +\gamma_{--}e^2e'^2+\lambda_{--}(\boldsymbol{e}.\boldsymbol{e'})^2+\kappa_{--}(\boldsymbol{e}.\boldsymbol{e'})e'^2
\end{aligned}$$

where

$$\alpha_{++}=\sqrt{\frac{G}{M_\bullet}}\left(\frac{1}{2{a_+}^{3/2}}\right){c_{20}^0}^{++} \qquad \beta_{++}=\sqrt{\frac{G}{M_\bullet}}\left(\frac{1}{2{a_+}^{3/2}}\right){c_{11}^1}^{++}$$

$$\gamma_{++}=\sqrt{\frac{G}{M_\bullet}}\left(\frac{1}{2{a_+}^{3/2}}\right)({c_{22}^0}^{++}-{c_{22}^2}^{++}) \qquad \lambda_{++}=\sqrt{\frac{G}{M_\bullet}}\left(\frac{1}{{a_+}^{3/2}}\right){c_{22}^2}^{++}$$

$$\kappa_{++}=\sqrt{\frac{G}{M_\bullet}}\left(\frac{1}{2{a_+}^{3/2}}\right){c_{13}^1}^{++} \qquad \chi_{++}=\sqrt{\frac{G}{M_\bullet}}\left(\frac{1}{2{a_+}^{3/2}}\right){c_{40}^0}^{++}$$

$$\nu_{++}=\sqrt{\frac{G}{M_\bullet}}\left(\frac{1}{2{a_+}^{3/2}}\right){c_{31}^1}^{++}$$

and

$$\alpha_{cp} = \sqrt{\frac{G}{M_\bullet}} \left(\frac{\sqrt{a_-}}{2{a_+}^2} \right) {c_{20}^0}^{+-} \qquad \alpha_{cm} = \sqrt{\frac{G}{M_\bullet}} \left(\frac{\sqrt{a_-}}{2{a_+}^2} \right) {c_{02}^0}^{+-}$$

$$\kappa_{cp} = \sqrt{\frac{G}{M_\bullet}} \left(\frac{\sqrt{a_-}}{2{a_+}^2} \right) {c_{31}^1}^{+-} \qquad \kappa_{cm} = \sqrt{\frac{G}{M_\bullet}} \left(\frac{\sqrt{a_-}}{2{a_+}^2} \right) {c_{13}^1}^{+-}$$

$$\beta_c = \sqrt{\frac{G}{M_\bullet}} \left(\frac{\sqrt{a_-}}{2{a_+}^2} \right) {c_{11}^1}^{+-} \qquad \gamma_c = \sqrt{\frac{G}{M_\bullet}} \left(\frac{\sqrt{a_-}}{2{a_+}^2} \right) ({c_{22}^0}^{+-} - {c_{22}^2}^{+-})$$

$$\lambda_c = \sqrt{\frac{G}{M_\bullet}} \left(\frac{\sqrt{a_-}}{{a_+}^2} \right) {c_{22}^2}^{+-} \qquad \chi_{cp} = \sqrt{\frac{G}{M_\bullet}} \left(\frac{\sqrt{a_-}}{2{a_+}^2} \right) {c_{40}^0}^{+-}$$

$$\chi_{cm} = \sqrt{\frac{G}{M_\bullet}} \left(\frac{\sqrt{a_-}}{2{a_+}^2} \right) {c_{04}^0}^{+-}$$

and

$$\alpha_{--} = \sqrt{\frac{G}{M_\bullet}} \left(\frac{1}{2{a_-}^{3/2}} \right) {c_{02}^0}^{--} \qquad \beta_{--} = \sqrt{\frac{G}{M_\bullet}} \left(\frac{1}{2{a_-}^{3/2}} \right) {c_{11}^1}^{--}$$

$$\gamma_{--} = \sqrt{\frac{G}{M_\bullet}} \left(\frac{1}{2{a_-}^{3/2}} \right) ({c_{22}^0}^{--} - {c_{22}^2}^{--}) \qquad \lambda_{--} = \sqrt{\frac{G}{M_\bullet}} \left(\frac{1}{{a_-}^{3/2}} \right) {c_{22}^2}^{--}$$

$$\kappa_{--} = \sqrt{\frac{G}{M_\bullet}} \left(\frac{1}{2{a_-}^{3/2}} \right) {c_{31}^1}^{--} \qquad \chi_{--} = \sqrt{\frac{G}{M_\bullet}} \left(\frac{1}{2{a_-}^{3/2}} \right) {c_{04}^0}^{--}$$

$$\nu_{--} = \sqrt{\frac{G}{M_\bullet}} \left(\frac{1}{2{a_-}^{3/2}} \right) {c_{13}^1}^{--}$$

Now, that we have the expressions of the interaction functions Ψs, we can substitute for them in the Hamiltonians. But before that, we would like to perform a change of variables to make things simpler: $(l,g) \rightarrow (x_+, y_+), (x_-, y_-)$, where we have assigned two separate

phase spaces for the prograde and retrograde populations [11]. The prograde population is presented in the $+$ phase space and the retrograde population is presented in the $-$ phase space.

Note that the (l,g) phase space is equivalent to two separate phase spaces; (e_+,g_+) for the prograde population and (e_-,g_-) for the retrograde population, where

$$e_+{}^2 = 1-l^2 \quad \text{and} \quad g_+ = g\,, \quad \text{for the prograde population.}$$

$$e_-{}^2 = 1-l^2 \quad \text{and} \quad g_- = g\,, \quad \text{for the retrograde population.}$$

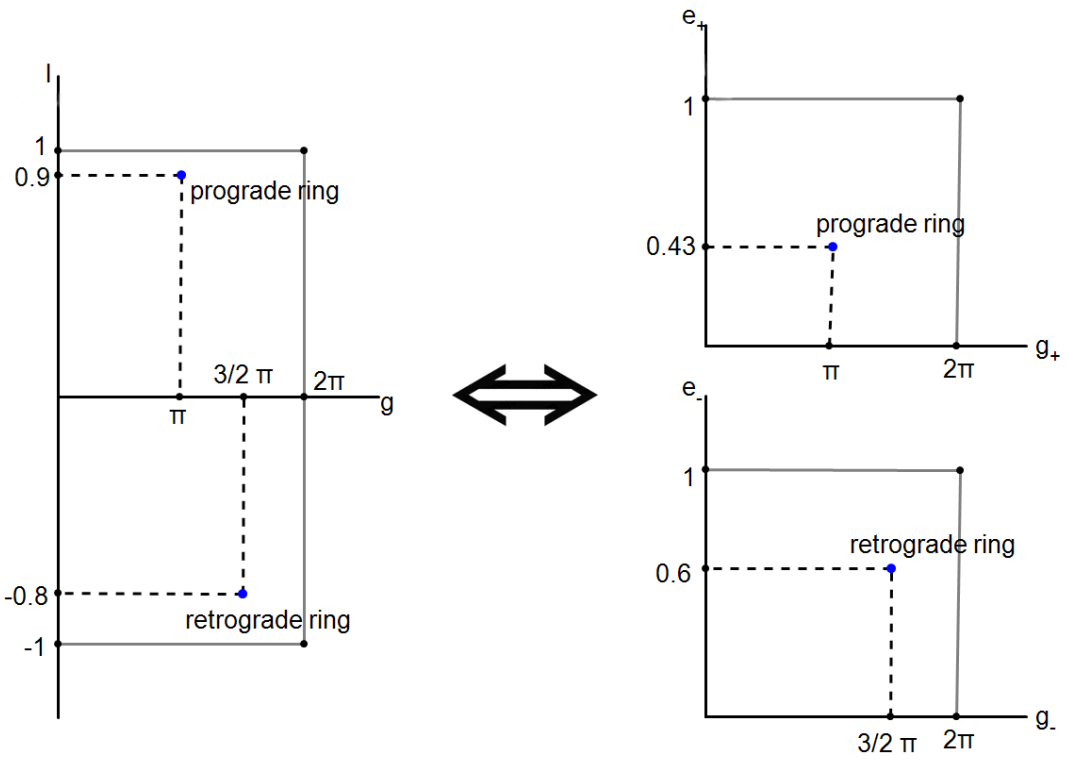

Figure 8: Equivalence of (l,g) phase space with (e_+,g_+) and (e_-,g_-) phase spaces.

From now on, we will relate any newly defined phase space to the (e_+,g_+) and (e_-,g_-) phase spaces. This will allow us to interpret any new variable in terms of well-known physical quantities; the eccentricity e and the orientation g. We transform now from

(e_+, g_+), (e_-, g_-) to (x_+, y_+), (x_-, y_-) where

$$\begin{aligned} {x_+}^2 + {y_+}^2 &\simeq {e_+}^2 \\ -x_+/y_+ &= \tan g_+ \\ {x_-}^2 + {y_-}^2 &\simeq {e_-}^2 \\ +x_-/y_- &= \tan g_- \end{aligned}$$

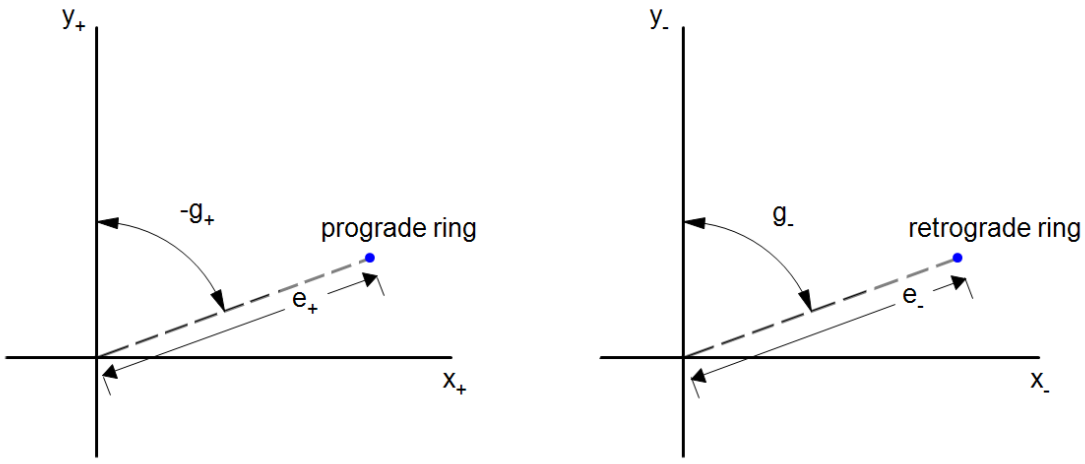

Figure 9: Meaning of e_+, g_+, e_- and g_- in the (x_+, y_+) and (x_-, y_-) phase spaces.

As a result:

$$f^+(l, g, t) \rightarrow f^+(x_+, y_+, t)$$

$$f^-(l, g, t) \rightarrow f^-(x_-, y_-, t)$$

$$\Psi(a_+, l, g; a_+, l', g') \rightarrow \Psi(x_+, y_+; x'_+, y'_+)$$

$$\Psi(a_+, l, g; a_-, l', g') \rightarrow \Psi(x_+, y_+; x'_-, y'_-)$$

$$\Psi(a_-, l, g; a_+, l', g') \rightarrow \Psi(x_-, y_-; x'_+, y'_+)$$

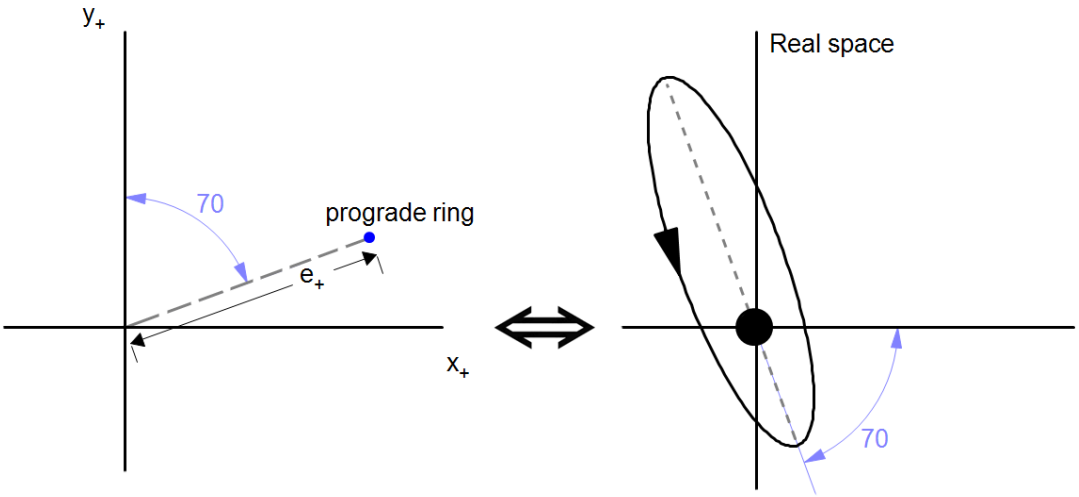

Figure 10: A point in the (x_+, y_+) phase space represents a prograde ring with specific eccentricity and orientation.

$$\Psi(a_-, l, g; a_-, l', g') \rightarrow \Psi(x_-, y_-; x'_-, y'_-)$$

$$H^+(l, g, t) \rightarrow H^+(x_+, y_+, t)$$

$$H^-(l, g, t) \rightarrow H^-(x_-, y_-, t)$$

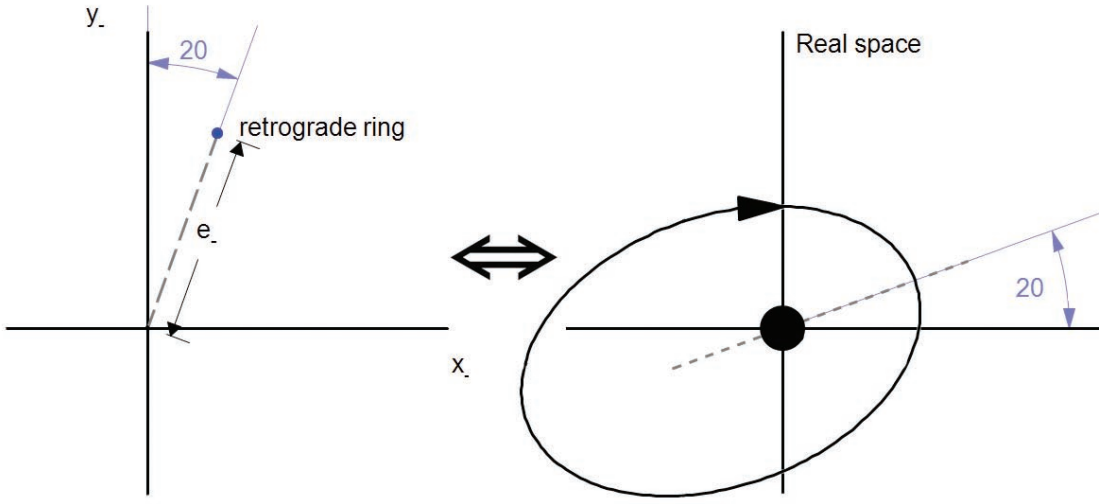

Figure 11: A point in the (x_-, y_-) phase space represents a retrograde ring with specific eccentricity and orientation.

The Hamiltonians are now given by:

$$\begin{aligned} H^+(x_+,y_+,t) &= -\int \mathrm{d}x'_+\mathrm{d}y'_+ \;\; f^+(x'_+,y'_+,t) \;\; \sqrt{\frac{G}{M_\bullet a_+}}\Psi(x_+,y_+;x'_+,y'_+) \\ &\quad -\int \mathrm{d}x'_-\mathrm{d}y'_- \;\; f^-(x'_-,y'_-,t) \;\; \sqrt{\frac{G}{M_\bullet a_+}}\Psi(x_+,y_+;x'_-,y'_-) \end{aligned}$$

and

$$\begin{aligned} H^-(x_-,y_-,t) &= -\int \mathrm{d}x'_+\mathrm{d}y'_+ \;\; f^+(x'_+,y'_+,t) \;\; \sqrt{\frac{G}{M_\bullet a_-}}\Psi(x_-,y_-;x'_+,y'_+) \\ &\quad -\int \mathrm{d}x'_-\mathrm{d}y'_- \;\; f^-(x'_-,y'_-,t) \;\; \sqrt{\frac{G}{M_\bullet a_-}}\Psi(x_-,y_-;x'_-,y'_-) \end{aligned}$$

where

$$\begin{aligned} \sqrt{\frac{G}{M_\bullet a_+}}\,\Psi(+,+') &= (\alpha_{++}+\gamma_{++}({x'_+}^2+{y'_+}^2)+\lambda_{++}{x'_+}^2){x_+}^2 + \\ &\quad (\alpha_{++}+\gamma_{++}({x'_+}^2+{y'_+}^2)+\lambda_{++}{y'_+}^2){y_+}^2 + \\ &\quad (2\lambda_{++}x'_+y'_+)x_+y_+ + \\ &\quad (\beta_{++}x'_+ + (\kappa_{++}-\frac{\beta_{++}}{8})x'_+({x'_+}^2+{y'_+}^2))x_+ + \\ &\quad (\beta_{++}y'_+ + (\kappa_{++}-\frac{\beta_{++}}{8})y'_+({x'_+}^2+{y'_+}^2))y_+ + \\ &\quad ((\nu_{++}-\frac{\beta_{++}}{8})x'_+)x_+({x_+}^2+{y_+}^2) + \\ &\quad ((\nu_{++}-\frac{\beta_{++}}{8})y'_+)y_+({x_+}^2+{y_+}^2) + \\ &\quad (\chi_{++}-\frac{\alpha_{++}}{4})({x_+}^2+{y_+}^2)^2 \end{aligned}$$

$$
\begin{aligned}
\sqrt{\frac{G}{M_\bullet a_+}}\,\Psi(+,-') \;=\; & \sqrt{\frac{a_-}{a_+}}\Big((\alpha_{cp}+\gamma_c({x'_-}^2+{y'_-}^2)+\lambda_c {x'_-}^2){x_+}^2+\\
& (\alpha_{cp}+\gamma_c({x'_-}^2+{y'_-}^2)+\lambda_c {y'_-}^2){y_+}^2-\\
& (2\lambda_c x'_- y'_-)x_+y_+-\\
& (\beta_c x'_-+(\kappa_{cm}-\frac{\beta_c}{8})x'_-({x'_-}^2+{y'_-}^2))x_+ +\\
& (\beta_c y'_-+(\kappa_{cm}-\frac{\beta_c}{8})y'_-({x'_-}^2+{y'_-}^2))y_+ -\\
& ((\kappa_{cp}-\frac{\beta_c}{8})x'_-)x_+({x_+}^2+{y_+}^2)+\\
& ((\kappa_{cp}-\frac{\beta_c}{8})y'_-)y_+({x_+}^2+{y_+}^2)+\\
& (\chi_{cp}-\frac{\alpha_{cp}}{4})({x_+}^2+{y_+}^2)^2\Big)
\end{aligned}
$$

$$
\begin{aligned}
\sqrt{\frac{G}{M_\bullet a_-}}\,\Psi(-,+') \;=\; & (\alpha_{cm}+\gamma_c({x'_+}^2+{y'_+}^2)+\lambda_c {x'_+}^2){x_-}^2+\\
& (\alpha_{cm}+\gamma_c({x'_+}^2+{y'_+}^2)+\lambda_c {y'_+}^2){y_-}^2-\\
& (2\lambda_c x'_+ y'_+)x_-y_--\\
& (\beta_c x'_++(\kappa_{cp}-\frac{\beta_c}{8})x'_+({x'_+}^2+{y'_+}^2))x_- +\\
& (\beta_c y'_++(\kappa_{cp}-\frac{\beta_c}{8})y'_+({x'_+}^2+{y'_+}^2))y_- -\\
& ((\kappa_{cm}-\frac{\beta_c}{8})x'_+)x_-({x_-}^2+{y_-}^2)+\\
& ((\kappa_{cm}-\frac{\beta_c}{8})y'_+)y_-({x_-}^2+{y_-}^2)+\\
& (\chi_{cm}-\frac{\alpha_{cm}}{4})({x_-}^2+{y_-}^2)^2
\end{aligned}
$$

$$\begin{aligned}\sqrt{\frac{G}{M_\bullet a_-}}\,\Psi(-,-') &= (\alpha_{--}+\gamma_{--}({x'_-}^2+{y'_-}^2)+\lambda_{--}{x'_-}^2){x_-}^2+\\ &\quad (\alpha_{--}+\gamma_{--}({x'_-}^2+{y'_-}^2)+\lambda_{--}{y'_-}^2){y_-}^2+\\ &\quad (2\lambda_{--}x'_-y'_-)x_-y_-+\\ &\quad (\beta_{--}x'_-+(\kappa_{--}-\frac{\beta_{--}}{8})x'_-({x'_-}^2+{y'_-}^2))x_-+\\ &\quad (\beta_{--}y'_-+(\kappa_{--}-\frac{\beta_{--}}{8})y'_-({x'_-}^2+{y'_-}^2))y_-+\\ &\quad ((\nu_{--}-\frac{\beta_{--}}{8})x'_-)x_-({x_-}^2+{y_-}^2)+\\ &\quad ((\nu_{--}-\frac{\beta_{--}}{8})y'_-)y_-({x_-}^2+{y_-}^2)+\\ &\quad (\chi_{--}-\frac{\alpha_{--}}{4})({x_-}^2+{y_-}^2)^2\end{aligned}$$

2. Ring Hamiltonian Expansion

In order to find the expressions of the Hamiltonians, we substitute for the Ψs in the Hamiltonians to get:

Prograde ring

$$\begin{aligned}H^+(x_+,y_+,t) &= \frac{1}{2}A_+x_+^2+B_+x_+y_++\frac{1}{2}C_+y_+^2+D_+x_++E_+y_+\\ &\quad +F_+x_+(x_+^2+y_+^2)+G_+y_+(x_+^2+y_+^2)+K_+(x_+^2+y_+^2)^2\end{aligned}$$

Retrograde ring

$$\begin{aligned}H^-(x_-,y_-,t) &= \frac{1}{2}A_-x_-^2+B_-x_-y_-+\frac{1}{2}C_-y_-^2+D_-x_-+E_-y_-\\ &\quad +F_-x_-(x_-^2+y_-^2)+G_-y_-(x_-^2+y_-^2)+K_-(x_-^2+y_-^2)^2\end{aligned}$$

where

$$
\begin{aligned}
A_+ &= -2\int dx_+dy_+\, f^+(x_+,y_+,t)\,\Big(\alpha_{++}+(\gamma_{++}+\lambda_{++})x_+^2+\gamma_{++}y_+^2\Big)\\
&\quad -2\sqrt{\frac{a_-}{a_+}}\int dx_-dy_-\, f^-(x_-,y_-,t)\,\Big(\alpha_{cp}+(\gamma_c+\lambda_c)x_-^2+\gamma_c y_-^2\Big)
\end{aligned}
$$

$$
\begin{aligned}
B_+ &= -2\lambda_{++}\int dx_+dy_+\, f^+(x_+,y_+,t)\,x_+y_+\\
&\quad +2\lambda_c\sqrt{\frac{a_-}{a_+}}\int dx_-dy_-\, f^-(x_-,y_-,t)\,x_-y_-
\end{aligned}
$$

$$
\begin{aligned}
C_+ &= -2\int dx_+dy_+\, f^+(x_+,y_+,t)\,\Big(\alpha_{++}+\gamma_{++}x_+^2+(\gamma_{++}+\lambda_{++})y_+^2\Big)\\
&\quad -2\sqrt{\frac{a_-}{a_+}}\int dx_-dy_-\, f^-(x_-,y_-,t)\,\Big(\alpha_{cp}+\gamma_c x_-^2+(\gamma_c+\lambda_c)y_-^2\Big)
\end{aligned}
$$

$$
\begin{aligned}
D_+ &= -\int dx_+dy_+\, f^+(x_+,y_+,t)\,\Big(\beta_{++}x_++(\kappa_{++}-\frac{\beta_{++}}{8})x_+(x_+^2+y_+^2)\Big)\\
&\quad +\sqrt{\frac{a_-}{a_+}}\int dx_-dy_-\, f^-(x_-,y_-,t)\,\Big(\beta_c x_-+(\kappa_{cm}-\frac{\beta_c}{8})x_-(x_-^2+y_-^2)\Big)
\end{aligned}
$$

$$
\begin{aligned}
E_+ &= -\int dx_+dy_+\, f^+(x_+,y_+,t)\,\Big(\beta_{++}y_++(\kappa_{++}-\frac{\beta_{++}}{8})y_+(x_+^2+y_+^2)\Big)\\
&\quad -\sqrt{\frac{a_-}{a_+}}\int dx_-dy_-\, f^-(x_-,y_-,t)\,\Big(\beta_c y_-+(\kappa_{cm}-\frac{\beta_c}{8})y_-(x_-^2+y_-^2)\Big)
\end{aligned}
$$

$$
\begin{aligned}
F_+ &= -\Big(\nu_{++}-\frac{\beta_{++}}{8}\Big)\int dx_+dy_+\, f^+(x_+,y_+,t)\,x_+\\
&\quad +\sqrt{\frac{a_-}{a_+}}\Big(\kappa_{cp}-\frac{\beta_c}{8}\Big)\int dx_-dy_-\, f^-(x_-,y_-,t)\,x_-
\end{aligned}
$$

$$
\begin{aligned}
G_+ &= -\Big(\nu_{++}-\frac{\beta_{++}}{8}\Big)\int dx_+dy_+\, f^+(x_+,y_+,t)\,y_+\\
&\quad -\sqrt{\frac{a_-}{a_+}}\Big(\kappa_{cp}-\frac{\beta_c}{8}\Big)\int dx_-dy_-\, f^-(x_-,y_-,t)\,y_-
\end{aligned}
$$

$$
\begin{aligned}
K_+ &= -\Big(\chi_{++} - \frac{\alpha_{++}}{4}\Big) \int dx_+ dy_+ \; f^+(x_+, y_+, t) \\
&\quad -\sqrt{\frac{a_-}{a_+}} \Big(\chi_{cp} - \frac{\alpha_{cp}}{4}\Big) \int dx_- dy_- \; f^-(x_-, y_-, t)
\end{aligned}
$$

and

$$
\begin{aligned}
A_- &= -2 \int dx_+ dy_+ \; f^+(x_+, y_+, t) \; \Big(\alpha_{cm} + (\gamma_c + \lambda_c) x_+^2 + \gamma_c y_+^2\Big) \\
&\quad -2 \int dx_- dy_- \; f^-(x_-, y_-, t) \; \Big(\alpha_{--} + (\gamma_{--} + \lambda_{--}) x_-^2 + \gamma_{--} y_-^2\Big)
\end{aligned}
$$

$$
\begin{aligned}
B_- &= 2\lambda_c \int dx_+ dy_+ \; f^+(x_+, y_+, t) \; x_+ y_+ \\
&\quad -2\lambda_{--} \int dx_- dy_- \; f^-(x_-, y_-, t) \; x_- y_-
\end{aligned}
$$

$$
\begin{aligned}
C_- &= -2 \int dx_+ dy_+ \; f^+(x_+, y_+, t) \; \Big(\alpha_{cm} + \gamma_c x_+^2 + (\gamma_c + \lambda_c) y_+^2\Big) \\
&\quad -2 \int dx_- dy_- \; f^-(x_-, y_-, t) \; \Big(\alpha_{--} + \gamma_{--} x_-^2 + (\gamma_{--} + \lambda_{--}) y_-^2\Big)
\end{aligned}
$$

$$
\begin{aligned}
D_- &= \int dx_+ dy_+ \; f^+(x_+, y_+, t) \; \Big(\beta_c x_+ + (\kappa_{cp} - \frac{\beta_c}{8}) x_+ (x_+^2 + y_+^2)\Big) \\
&\quad - \int dx_- dy_- \; f^-(x_-, y_-, t) \; \Big(\beta_{--} x_- + (\kappa_{--} - \frac{\beta_{--}}{8}) x_- (x_-^2 + y_-^2)\Big)
\end{aligned}
$$

$$
\begin{aligned}
E_- &= - \int dx_+ dy_+ \; f^+(x_+, y_+, t) \; \Big(\beta_c y_+ + (\kappa_{cp} - \frac{\beta_c}{8}) y_+ (x_+^2 + y_+^2)\Big) \\
&\quad - \int dx_- dy_- \; f^-(x_-, y_-, t) \; \Big(\beta_{--} y_- + (\kappa_{--} - \frac{\beta_{--}}{8}) y_- (x_-^2 + y_-^2)\Big)
\end{aligned}
$$

$$
\begin{aligned}
F_- &= \Big(\kappa_{cm} - \frac{\beta_c}{8}\Big) \int dx_+ dy_+ \; f^+(x_+, y_+, t) \; x_+ \\
&\quad -\Big(\nu_{--} - \frac{\beta_{--}}{8}\Big) \int dx_- dy_- \; f^-(x_-, y_-, t) \; x_-
\end{aligned}
$$

$$
\begin{aligned}
G_- &= -\Big(\kappa_{cm} - \frac{\beta_c}{8}\Big) \int dx_+ dy_+ \; f^+(x_+, y_+, t)\; y_+ \\
&\quad -\Big(\nu_{--} - \frac{\beta_{--}}{8}\Big) \int dx_- dy_- \; f^-(x_-, y_-, t)\; y_-
\end{aligned}
$$

$$
\begin{aligned}
K_- &= -\Big(\chi_{cm} - \frac{\alpha_{cm}}{4}\Big) \int dx_+ dy_+ \; f^+(x_+, y_+, t) \\
&\quad -\Big(\chi_{--} - \frac{\alpha_{--}}{4}\Big) \int dx_- dy_- \; f^-(x_-, y_-, t)
\end{aligned}
$$

So, H^+ and H^- are 4^{th} order Hamiltonians given in terms of f^+ and f^-. Hence, once we know the distribution functions, we can substitute for them and calculate H^+ and H^- of the system.

E. Constructing the distribution function

Consider a collisionless system of stars in a steady state. This means that the distribution function and the potential (or the Hamiltonian) corresponding to this system are both explicitly independent of time. On the other hand, we know from the collisionless Boltzmann equation, $\frac{\mathrm{df}}{\mathrm{dt}} = 0$, that the distribution function is constant along the phase space trajectories. From what preceded, we can infer that star trajectories map out constant values of the distribution function. In other words, the distribution function can be constructed by taking it as a function of phase space trajectories.

Phase space trajectories can be found through isolating integrals of motion. An integral of motion is by definition a function of the phase space only (no explicit time dependence) which is constant along trajectories [12]. Sometimes the integral of motion can isolate orbits in the phase space. In this case, the integral of motion would be called isolating integral of motion. If we take the distribution function as a function of an isolating integral, this distribution function would be a solution of the collisionless Boltzmann equation governing the system and would constitute the right representation of the system of stars. In our case, our system is not in a steady state, instead it is evolving slowly in time. There-

fore, The distribution function and the Hamiltonian are both function of time. Nevertheless, the above discussion can still be applied as an approximate case for small intervals of time. This allows us to find an approximate time-dependent invariant that does the job of isolating integrals for small intervals of time. This invariant, in turn, would allow us to find a time-dependent distribution function for our system.

1. An approximate invariant

To make thing simpler, we prefer to deal with a quadratic Hamiltonian because it leads to a linear dynamics. First, it's always possible to get rid of the linear terms by shifting the origin of the phase space to a new movable origin satisfying certain conditions. We take the new origin to be $(X(t),Y(t))$ such that $X(t)$ and $Y(t)$ satisfy the following four equations:

$$\begin{aligned}
\frac{\mathrm{d}X_+}{\mathrm{d}t} &= B_+X_+ + C_+Y_+ + E_+ + 2F_+X_+Y_+ + G_+(X_+^2 + 3Y_+^2) + 4K_+(Y_+^3 + Y_+X_+^2) \\
\frac{\mathrm{d}Y_+}{\mathrm{d}t} &= -A_+X_+ - B_+Y_+ - D_+ - F_+(3X_+^2 + Y_+^2) - 2G_+X_+Y_+ - 4K_+(X_+^3 + X_+Y_+^2) \\
\frac{\mathrm{d}X_-}{\mathrm{d}t} &= B_-X_- + C_-Y_- + E_- + 2F_-X_-Y_- + G_-(X_-^2 + 3Y_-^2) + 4K_-(Y_-^3 + Y_-X_-^2) \\
\frac{\mathrm{d}Y_-}{\mathrm{d}t} &= -A_-X_- - B_-Y_- - D_- - F_-(3X_-^2 + Y_-^2) - 2G_-X_-Y_- - 4K_-(X_-^3 + X_-Y_-^2)
\end{aligned}$$

The change of variables presenting the origin shift is given by

$$\begin{aligned}
\xi_1 &= x - X(t) \\
\xi_2 &= y - Y(t)
\end{aligned}$$

Now our Hamiltonians in the new phase space have no linear terms any more. Second, suppose that the distribution functions are restricted to a small region around the new origins. This implies that we are dealing with (x,y) very close to the new origins (X,Y), or equivalently very small ξ. As a result, we can neglect any term in the Hamiltonian

higher than the quadratic terms. So after the above change of variables and under the condition of small ξs, we can consider our Hamiltonian to be quadratic and our dynamics to be linear.

2. Determining an invariant J for a linear system

Consider a linear system that possesses a quadratic Hamiltonian $H(\xi_1, \xi_2)$, we can always write H as

$$H = \frac{1}{2} A \ {\xi_1}^2 + \frac{1}{2} C \ {\xi_2}^2 + B \ \xi_1 \xi_2$$

Hence the linear equations of motion (from Hamilton's equations) will be given by

$$\begin{aligned} \dot{\xi_1} &= B \ \xi_1 + C \ \xi_2 \\ \dot{\xi_2} &= -A \ \xi_1 - B \ \xi_2 \end{aligned}$$

Or in a matrix form:

$$\dot{\xi} = T \ \xi$$

where

$$\xi = \begin{pmatrix} \xi_1 \\ \xi_2 \end{pmatrix} \quad \text{and} \quad T = \begin{pmatrix} B & C \\ -A & -B \end{pmatrix}$$

Take the function $J(\xi_1, \xi_2)$ given by

$$J = \frac{1}{2} \ \xi^T \ Q \ \xi$$

where Q is a 2×2 matrix such that $\frac{\mathrm{d}(\det Q)}{\mathrm{d}t} = 0$.

$$\frac{\mathrm{d}J}{\mathrm{d}t} = \frac{1}{2} \ \xi^T \left(T^T \ Q + \frac{\mathrm{d}Q}{\mathrm{d}t} + Q \ T \right) \xi = 0$$

Thus J is an invariant of the motion. It is a function of the phase space (ξ_1, ξ_2) with its isocontours are ellipses centered on the origin.

The distribution function should be chosen now to be a function of the approximate invariant J. At any instant of time, the isocontours of the distribution function are ellipses that are centered on (X,Y) which can be considered as the coordinates of the centroids of the distribution function, in the (x,y) phase space. Those isocontours (the ellipses) evolve in time in the phase space and change shapes and orientations.

Let us finally state precisely the conditions under which this distribution function is an approximate solution:

1. The dispersions in the eccentricities are much smaller than their centroid values. (the DFs f^+ and f^- are delta functions at the centroids)

2. The interval of time, we are dealing with, is relatively small.

F. Final Form of the Ring Hamiltonian

Now that we have the distribution functions as delta functions at the centroids (X_+, Y_+) and (X_-, Y_-), we can do the integrations and recover final expressions of the coefficients $A_\pm, B_\pm, C_\pm, D_\pm, E_\pm, F_\pm, G_\pm$ and $K_\pm$. Hence:

Prograde ring

$$\begin{aligned} H^+(x_+, y_+, t) &= \frac{1}{2}A_+{x_+}^2 + B_+x_+y_+ + \frac{1}{2}C_+{y_+}^2 + D_+x_+ + E_+y_+ \\ &\quad + F_+x_+({x_+}^2 + {y_+}^2) + G_+y_+({x_+}^2 + {y_+}^2) + K_+({x_+}^2 + {y_+}^2)^2 \end{aligned}$$

Retrograde ring

$$\begin{aligned} H^-(x_-, y_-, t) &= \frac{1}{2}A_-{x_-}^2 + B_-x_-y_- + \frac{1}{2}C_-{y_-}^2 + D_-x_- + E_-y_- \\ &\quad + F_-x_-({x_-}^2 + {y_-}^2) + G_-y_-({x_-}^2 + {y_-}^2) + K_-({x_-}^2 + {y_-}^2)^2 \end{aligned}$$

where

$$
\begin{aligned}
A_+ &= -2M_+\Big(\alpha_{++}+(\gamma_{++}+\lambda_{++}){X_+}^2+\gamma_{++}{Y_+}^2\Big)\\
&\quad -2M_-\sqrt{\frac{a_-}{a_+}}\,\Big(\alpha_{cp}+(\gamma_c+\lambda_c){X_-}^2+\gamma_c{Y_-}^2\Big)
\end{aligned}
$$

$$
B_+ = -2\lambda_{++}M_+X_+Y_+ \;+\; 2\lambda_cM_-\sqrt{\frac{a_-}{a_+}}\,X_-Y_-
$$

$$
\begin{aligned}
C_+ &= -2M_+\Big(\alpha_{++}+\gamma_{++}{X_+}^2+(\gamma_{++}+\lambda_{++}){Y_+}^2\Big)\\
&\quad -2M_-\sqrt{\frac{a_-}{a_+}}\,\Big(\alpha_{cp}+\gamma_c{X_-}^2+(\gamma_c+\lambda_c){Y_-}^2\Big)
\end{aligned}
$$

$$
\begin{aligned}
D_+ &= -M_+\Big(\beta_{++}X_+ + (\kappa_{++}-\frac{\beta_{++}}{8})X_+({X_+}^2+{Y_+}^2)\Big)\\
&\quad +M_-\sqrt{\frac{a_-}{a_+}}\,\Big(\beta_cX_- + (\kappa_{cm}-\frac{\beta_c}{8})X_-({X_-}^2+{Y_-}^2)\Big)
\end{aligned}
$$

$$
\begin{aligned}
E_+ &= -M_+\Big(\beta_{++}Y_+ + (\kappa_{++}-\frac{\beta_{++}}{8})Y_+({X_+}^2+{Y_+}^2)\Big)\\
&\quad -M_-\sqrt{\frac{a_-}{a_+}}\,\Big(\beta_cY_- + (\kappa_{cm}-\frac{\beta_c}{8})Y_-({X_-}^2+{Y_-}^2)\Big)
\end{aligned}
$$

$$
F_+ = -\Big(\nu_{++}-\frac{\beta_{++}}{8}\Big)M_+X_+ + \sqrt{\frac{a_-}{a_+}}\,\Big(\kappa_{cp}-\frac{\beta_c}{8}\Big)M_-X_-
$$

$$
G_+ = -\Big(\nu_{++}-\frac{\beta_{++}}{8}\Big)M_+Y_+ - \sqrt{\frac{a_-}{a_+}}\,\Big(\kappa_{cp}-\frac{\beta_c}{8}\Big)M_-Y_-
$$

$$
K_+ = -\Big(\chi_{++}-\frac{\alpha_{++}}{4}\Big)M_+ - \sqrt{\frac{a_-}{a_+}}\,\Big(\chi_{cp}-\frac{\alpha_{cp}}{4}\Big)M_-
$$

and

$$
\begin{aligned}
A_- &= -2M_+\Big(\alpha_{cm}+(\gamma_c+\lambda_c){X_+}^2+\gamma_c{Y_+}^2\Big)\\
&\quad -2M_-\Big(\alpha_{--}+(\gamma_{--}+\lambda_{--}){X_-}^2+\gamma_{--}{Y_-}^2\Big)
\end{aligned}
$$

$$
B_- = 2\lambda_c M_+X_+Y_+ - 2\lambda_{--}M_-X_-Y_-
$$

$$
\begin{aligned}
C_- &= -2M_+\Big(\alpha_{cm}+\gamma_c{X_+}^2+(\gamma_c+\lambda_c){Y_+}^2\Big)\\
&\quad -2M_-\Big(\alpha_{--}+\gamma_{--}{X_-}^2+(\gamma_{--}+\lambda_{--}){Y_-}^2\Big)
\end{aligned}
$$

$$
\begin{aligned}
D_- &= M_+\Big(\beta_cX_+ +(\kappa_{cp}-\frac{\beta_c}{8})X_+({X_+}^2+{Y_+}^2)\Big)\\
&\quad -M_-\Big(\beta_{--}X_- +(\kappa_{--}-\frac{\beta_{--}}{8})X_-({X_-}^2+{Y_-}^2)\Big)
\end{aligned}
$$

$$
\begin{aligned}
E_- &= -M_+\Big(\beta_cY_+ +(\kappa_{cp}-\frac{\beta_c}{8})Y_+({X_+}^2+{Y_+}^2)\Big)\\
&\quad -M_-\Big(\beta_{--}Y_- +(\kappa_{--}-\frac{\beta_{--}}{8})Y_-({X_-}^2+{Y_-}^2)\Big)
\end{aligned}
$$

$$
F_- = \Big(\kappa_{cm}-\frac{\beta_c}{8}\Big)M_+X_+ -\Big(\nu_{--}-\frac{\beta_{--}}{8}\Big)M_-X_-
$$

$$
G_- = -\Big(\kappa_{cm}-\frac{\beta_c}{8}\Big)M_+Y_+ -\Big(\nu_{--}-\frac{\beta_{--}}{8}\Big)M_-Y_-
$$

$$
K_- = -\Big(\chi_{cm}-\frac{\alpha_{cm}}{4}\Big)M_+ -\Big(\chi_{--}-\frac{\alpha_{--}}{4}\Big)M_-
$$

CHAPTER IV

CENTROID DYNAMICS

The system we were studying so far consisted of two populations of elliptical rings evolving in a plane while focused at the same point. The first population is prograde and has semi-major axis a_+ and the second population is retrograde and has semi-major axis a_-.

This system is represented by the distribution functions f^+ and f^- in the phase spaces (x_+, y_+) and (x_-, y_-) respectively. As shown before, f^+ has the centroid (X_+, Y_+) and f^- has the centroid (X_-, Y_-). The isocontours of f^+ and f^- are ellipses centered at their centroids. As the distribution functions evolve in time, the centroids move and the isocontours change shape and orientation.

The whole dynamics of the distribution functions can be described by the matrix Q driving the shape and orientation of the isocontours and the four equations describing the dynamics of the two centroids [11]. Since the distribution functions in our case were taken to be delta functions (i.e. the dispersion in eccentricities is much smaller than the centroid eccentricities), the shape and orientation dynamics is driven by the centroid dynamics and can be recovered from it. Hence we neglect any dynamics related to the shape or orientation of the distribution functions and focus on the centroid dynamics, the dynamics of two counter-rotating centroids.

As shown before, centroid dynamics is governed by the four equations:

$$\begin{aligned}
\frac{\mathrm{d}X_+}{\mathrm{d}t} &= +B_+X_+ + C_+Y_+ + E_+ + 2F_+X_+Y_+ + G_+(X_+^2 + 3Y_+^2) + 4K_+(Y_+^3 + Y_+X_+^2) \\
\frac{\mathrm{d}Y_+}{\mathrm{d}t} &= -A_+X_+ - B_+Y_+ - D_+ - F_+(3X_+^2 + Y_+^2) - 2G_+X_+Y_+ - 4K_+(X_+^3 + X_+Y_+^2) \\
\frac{\mathrm{d}X_-}{\mathrm{d}t} &= +B_-X_- + C_-Y_- + E_- + 2F_-X_-Y_- + G_-(X_-^2 + 3Y_-^2) + 4K_-(Y_-^3 + Y_-X_-^2) \\
\frac{\mathrm{d}Y_-}{\mathrm{d}t} &= -A_-X_- - B_-Y_- - D_- - F_-(3X_-^2 + Y_-^2) - 2G_-X_-Y_- - 4K_-(X_-^3 + X_-Y_-^2)
\end{aligned}$$

where the coefficients $A_\pm, B_\pm, C_\pm, D_\pm, E_\pm, F_\pm, G_\pm, K_\pm$ are given in (...). This system of four equations can be transformed to a two-degree-of-freedom Hamiltonian system by the following change of variables:

$$\begin{aligned} u_+ &= \mu_+^{\frac{1}{2}} a_+^{\frac{1}{4}} X_+ \\ v_+ &= \mu_+^{\frac{1}{2}} a_+^{\frac{1}{4}} Y_+ \\ u_- &= \mu_-^{\frac{1}{2}} a_-^{\frac{1}{4}} X_- \\ v_- &= \mu_-^{\frac{1}{2}} a_-^{\frac{1}{4}} Y_- \end{aligned}$$

To get a clear sense of the new variables u_+, v_+, u_- and v_-, we relate them to the eccentricity e_+^{c} and the orientation g_+^{c} of the prograde centroid and the eccentricity e_-^{c} and the orientation g_-^{c} of the retrograde centroid. (Fig. 12)

$$\begin{aligned} {u_+}^2 + {v_+}^2 &= \mu_+ \sqrt{a_+} {e_+^c}^2 \\ -u_+/v_+ &= \tan g_+^c \\ {u_-}^2 + {v_-}^2 &= \mu_- \sqrt{a_-} {e_-^c}^2 \\ +u_-/v_- &= \tan g_-^{\mathrm{c}} \end{aligned}$$

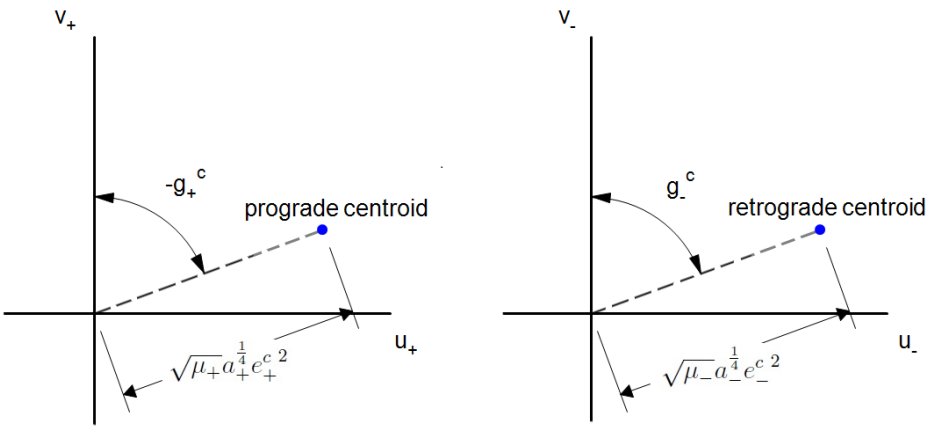

Figure 12: Meaning of e_+^{c}, g_+^{c}, e_-^{c} and g_-^{c} in the (u_+, v_+) and (u_-, v_-) phase spaces of counter-rotating centroids.

After substituting for the new variables in the four equations, one can show that the resulting system is an exact system. Performing the usual method of "partial integrations", we get the following full centroid Hamiltonian:

$$
\begin{aligned}
H \;=\; & -\left(M_+\left(\alpha_{++}+\frac{\beta_{++}}{2}\right)+M_-\sqrt{\frac{a_-}{a_+}}\alpha_{cp}\right)\left(u_+^2+v_+^2\right) \\
& -\left(M_-\left(\alpha_{--}+\frac{\beta_{--}}{2}\right)+M_+\alpha_{cm}\right)\left(u_-^2+v_-^2\right) \\
& +\beta_c\sqrt{M_+M_-}\left(\frac{a_-}{a_+}\right)^{\frac{1}{4}}\left(u_+u_--v_+v_-\right) \\
& -\left(M_-\frac{\sqrt{a_-}}{a_+\mu_+}\left(\chi_{cp}-\frac{\alpha_{cp}}{4}\right)\right. \\
& \left.+\frac{M}{\sqrt{a_+}}\left(\chi_{++}-\frac{\alpha_{++}}{4}+\frac{\kappa_{++}}{4}+\frac{3\nu_{++}}{4}-\frac{\beta_{++}}{8}+\frac{\gamma_{++}+\lambda_{++}}{2}\right)\right)\left(u_+^2+v_+^2\right)^2 \\
& -\left(M_+\frac{1}{\sqrt{a_-}\mu_-}\left(\chi_{cm}-\frac{\alpha_{cm}}{4}\right)\right. \\
& \left.+\frac{M}{\sqrt{a_-}}\left(\chi_{--}-\frac{\alpha_{--}}{4}+\frac{\kappa_{--}}{4}+\frac{3\nu_{--}}{4}-\frac{\beta_{--}}{8}+\frac{\gamma_{--}+\lambda_{--}}{2}\right)\right)\left(u_-^2+v_-^2\right)^2 \\
& -\frac{M}{\sqrt{a_+}}\gamma_c\left(u_+^2+v_+^2\right)\left(u_-^2+v_-^2\right)-\frac{M}{\sqrt{a_+}}\lambda_c\left(u_+u_--v_+v_-\right)^2 \\
& +\left(Ma_+^{-\frac{3}{4}}a_-^{\frac{1}{4}}\sqrt{\frac{\mu_-}{\mu_+}}\left(\kappa_{cp}-\frac{\beta_c}{8}\right)\left(u_+^2+v_+^2\right)\right. \\
& \left.+M\left(a_+a_-\right)^{-\frac{1}{4}}\sqrt{\frac{\mu_+}{\mu_-}}\left(\kappa_{cm}-\frac{\beta_c}{8}\right)\left(u_-^2+v_-^2\right)\right)\left(u_+u_--v_+v_-\right)
\end{aligned}
$$

A. Linearized Dynamics of Counter-rotating Centroids

when linearized, the four equations governing the dynamics of centroids become:

$$\begin{aligned}
\frac{\mathrm{d}u_+}{\mathrm{d}t} &= -2\left(M_+\left(\alpha_{++}+\frac{\beta_{++}}{2}\right)+M_-\sqrt{\frac{a_-}{a_+}}\alpha_{cp}\right)v_+ - \beta_c\sqrt{M_+M_-}\left(\frac{a_-}{a_+}\right)^{\frac{1}{4}}v_- \\
\frac{\mathrm{d}v_+}{\mathrm{d}t} &= +2\left(M_+\left(\alpha_{++}+\frac{\beta_{++}}{2}\right)+M_-\sqrt{\frac{a_-}{a_+}}\alpha_{cp}\right)u_+ - \beta_c\sqrt{M_+M_-}\left(\frac{a_-}{a_+}\right)^{\frac{1}{4}}u_- \\
\frac{\mathrm{d}u_-}{\mathrm{d}t} &= -2\left(M_-\left(\alpha_{--}+\frac{\beta_{--}}{2}\right)+M_+\alpha_{cm}\right)v_- - \beta_c\sqrt{M_+M_-}\left(\frac{a_-}{a_+}\right)^{\frac{1}{4}}v_+ \\
\frac{\mathrm{d}v_-}{\mathrm{d}t} &= +2\left(M_-\left(\alpha_{--}+\frac{\beta_{--}}{2}\right)+M_+\alpha_{cm}\right)u_- - \beta_c\sqrt{M_+M_-}\left(\frac{a_-}{a_+}\right)^{\frac{1}{4}}u_+
\end{aligned}$$

The underlying Hamiltonian is given by:

$$\begin{aligned}
H &= -\left(M_+\left(\alpha_{++}+\frac{\beta_{++}}{2}\right)+M_-\sqrt{\frac{a_-}{a_+}}\alpha_{cp}\right)\left(u_+^2+v_+^2\right) \\
&\quad -\left(M_-\left(\alpha_{--}+\frac{\beta_{--}}{2}\right)+M_+\alpha_{cm}\right)\left(u_-^2+v_-^2\right) \\
&\quad +\beta_c\sqrt{M_+M_-}\left(\frac{a_-}{a_+}\right)^{\frac{1}{4}}\left(u_+u_- - v_+v_-\right)
\end{aligned}$$

We can study the linear dynamics of centroids by directly studying the four corresponding linearized equations of motion. These four equations can be written as:

$$\begin{aligned}
\frac{\mathrm{d}u_+}{\mathrm{d}t} &= -\omega_+v_+ - \omega_c v_- \\
\frac{\mathrm{d}v_+}{\mathrm{d}t} &= +\omega_+u_+ - \omega_c u_- \\
\frac{\mathrm{d}u_-}{\mathrm{d}t} &= -\omega_-v_- - \omega_c v_+ \\
\frac{\mathrm{d}v_-}{\mathrm{d}t} &= +\omega_-u_- - \omega_c u_+
\end{aligned}$$

where

$$\begin{aligned}
\omega_+ &= 2\left(M_+\left(\alpha_{++}+\frac{\beta_{++}}{2}\right)+M_-\sqrt{\frac{a_-}{a_+}}\alpha_{cp}\right)\\
\omega_- &= 2\left(M_-\left(\alpha_{--}+\frac{\beta_{--}}{2}\right)+M_+\alpha_{cm}\right)\\
\omega_c &= \beta_c\sqrt{M_+M_-}\left(\frac{a_-}{a_+}\right)^{\frac{1}{4}}
\end{aligned}$$

In the phase space (u_+, v_+, u_-, v_-), the point $(0,0,0,0)$ is an equilibrium point that gives

$$\frac{\mathrm{d}u_+}{\mathrm{d}t}=\frac{\mathrm{d}v_+}{\mathrm{d}t}=\frac{\mathrm{d}u_-}{\mathrm{d}t}=\frac{\mathrm{d}v_-}{\mathrm{d}t}=0$$

At the level of centroids, this equilibrium point represents a zero-eccentricity equilibrium where the prograde and the retrograde centroids are circles of radius a_+ and a_- respectively. In this state, all the prograde stars move on the same circular orbit of radius a_+ and all the retrograde stars move on the same circular orbit of radius a_-.

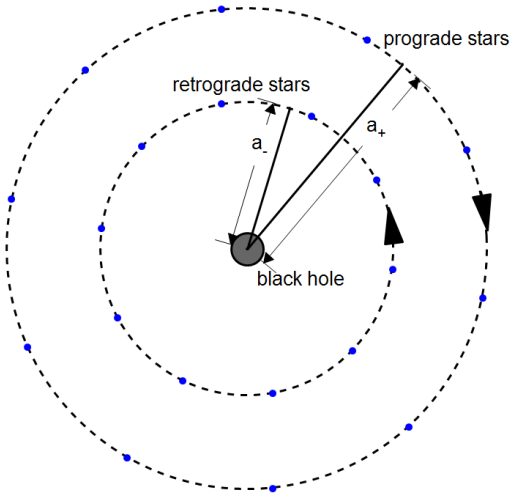

Figure 13: Orbits of prograde and retrograde stars at the zero-eccentricity equilibrium.

To find the nature of the zero-eccentricity equilibrium point, we have to study the behavior of the system around this point by studying the four linearized equations.

Using the complex notation $z_+ = u_+ + iv_+$ and $z_- = v_- + iu_-$, the 4 equations become:

$$\begin{aligned} \frac{\mathrm{d}z_+}{\mathrm{d}t} &= +i\omega_+ z_+ - \omega_c z_- \\ \frac{\mathrm{d}z_-}{\mathrm{d}t} &= -i\omega_- z_- - \omega_c z_+ \end{aligned}$$

Now take $z_+ = Z_+ e^{st}$ and $z_- = Z_- e^{st}$, we get:

$$\begin{aligned} sZ_+ &= +i\omega_+ Z_+ - \omega_c Z_- \\ sZ_- &= -i\omega_- Z_- - \omega_c Z_+ \end{aligned}$$

Or in a matrix form:

$$s \begin{pmatrix} Z_+ \\ Z_- \end{pmatrix} = \begin{pmatrix} i\omega_+ & -\omega_c \\ -\omega_c & -i\omega_- \end{pmatrix} \begin{pmatrix} Z_+ \\ Z_- \end{pmatrix}$$

$$\implies \det \begin{pmatrix} i\omega_+ - s & -\omega_c \\ -\omega_c & -i\omega_- - s \end{pmatrix} = 0$$

$$\implies s^2 + i(\omega_- - \omega_+)s + \omega_+\omega_- - {\omega_c}^2 = 0$$

The roots of this equation are given by

$$\begin{aligned} s_1 &= \frac{-i(\omega_- - \omega_+) + \sqrt{4{\omega_c}^2 - (\omega_+ + \omega_-)^2}}{2} \\ s_2 &= \frac{-i(\omega_- - \omega_+) - \sqrt{4{\omega_c}^2 - (\omega_+ + \omega_-)^2}}{2} \end{aligned}$$

If s_1 or s_2 is pure imaginary, the solutions will be periodic around the zero-eccentricity equilibrium point, which will then be a stable center point. On the other hand, if s_1 is not pure imaginary, then the real part would be positive and growing solutions would be allowed around the zero-eccentricity equilibrium point which will then be an unstable

point. Finally, if s_2 is not pure imaginary, then its real part would be negative in this case, and damped solutions would be allowed around the zero-eccentricity equilibrium point which will then be again an unstable point.

From what preceded, we know that the condition of instability of the zero-eccentricity equilibrium is given by

$$4{\omega_c}^2 - (\omega_+ + \omega_-)^2 > 0$$

This inequality can be written in terms of ρ, μ and b where $\rho = a_-/a_+$ is the semi-major axis ratio of the retrograde to the prograde orbits, $\mu = M_-/M_+$ is the mass ratio of the retro population to the pro population and b is the softening factor where the point-particle Newtonian potential $-\frac{GM^2}{r}$ is replaced by the following softened potential $-\frac{GM^2}{(r^2+b^2)^{\frac{1}{2}}}$. Softening is usually used to remove the singularity of the $\frac{1}{r^2}$ force and diminish the effect of graininess caused by treating the stars as point particles [13]. For too small softening, the estimated forces will be too noisy while for too large softening, the estimated forces are misrepresented. There is always an optimal softening that best represents the true forces in the system. The value of this optimal softening depends on the number of particles and the mass distribution in the system.

Therefore, ρ, μ and b are the only parameters that control the linear dynamics of centroids. The instability inequality is satisfied when μ is between the two roots of the equation. In figure 14, we plot the roots of the equation as a function of b for different values of ρ. The region between the curves (above the blue and below the red) corresponds to the instability of the zero-eccentricity equilibrium and describes uniformly precessing centroids of growing or damped eccentricities. On the other hand, the remaining region of figure 14 corresponds to the stability of the zero-eccentricity equilibrium and describes uniformly precessing centroids of fixed eccentricities.

The instability of the zero-eccentricity equilibrium operates through interactions between the prograde and the retrograde populations. For the instability to kick in through population interactions, the mass ratio μ of the prograde and the retrograde populations has to overcome certain critical values which depends on the softening b. One can also see

from figure 14 that the instability region depends also on the semi-major axis ratio ρ. For instance, the instability region gets smaller and smaller when ρ decreases.

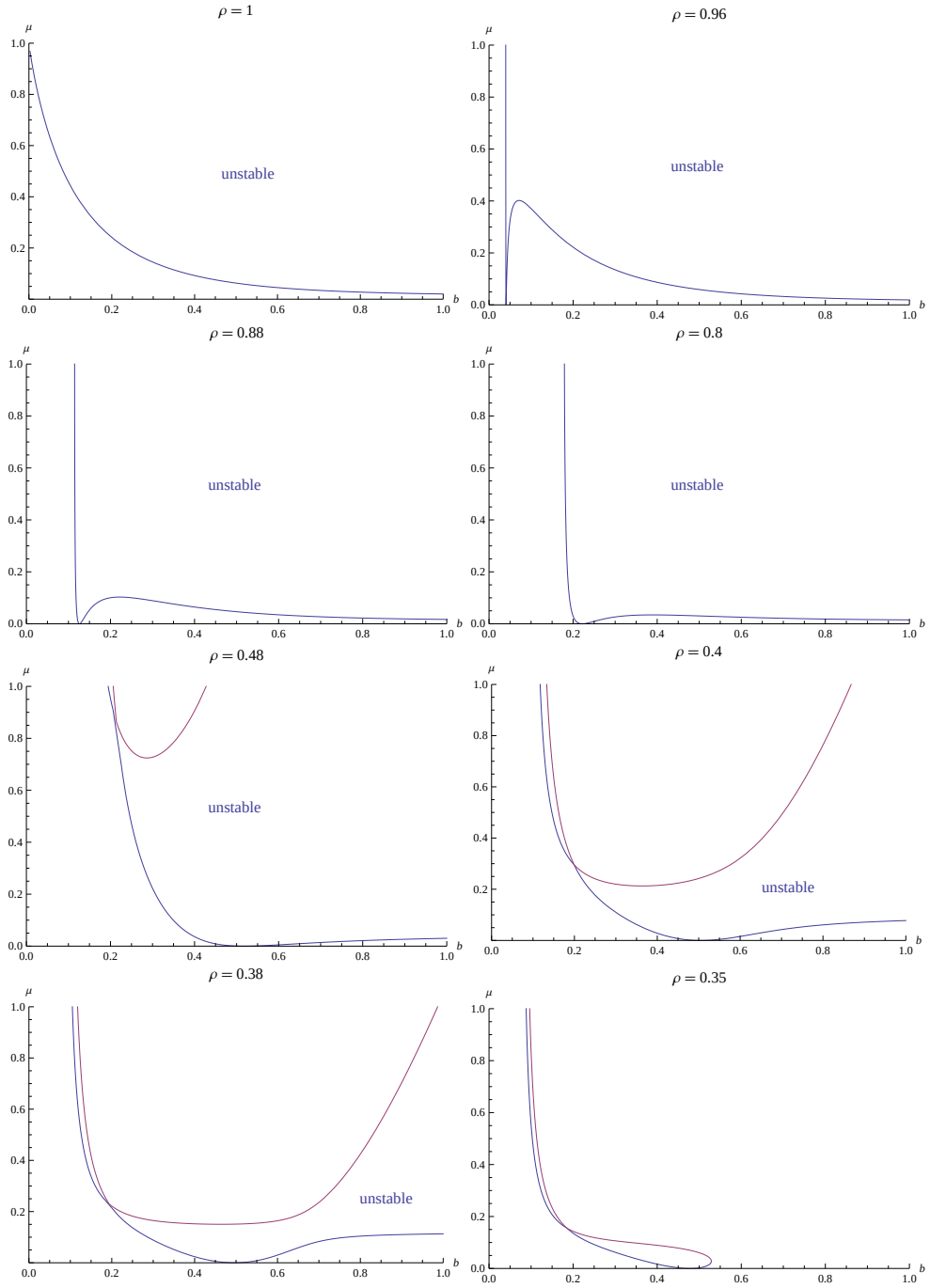

Figure 14: Linear instability regions for the zero-eccentricity equilibrium of counter-rotating centroids: Plots of μ as a function of b for different values of ρ

To focus more on the effect of the semi-major axis ratio ρ in the linear dynamics,

we plot in the figure 15 the plane of b and ρ for different values of μ. As shown in the

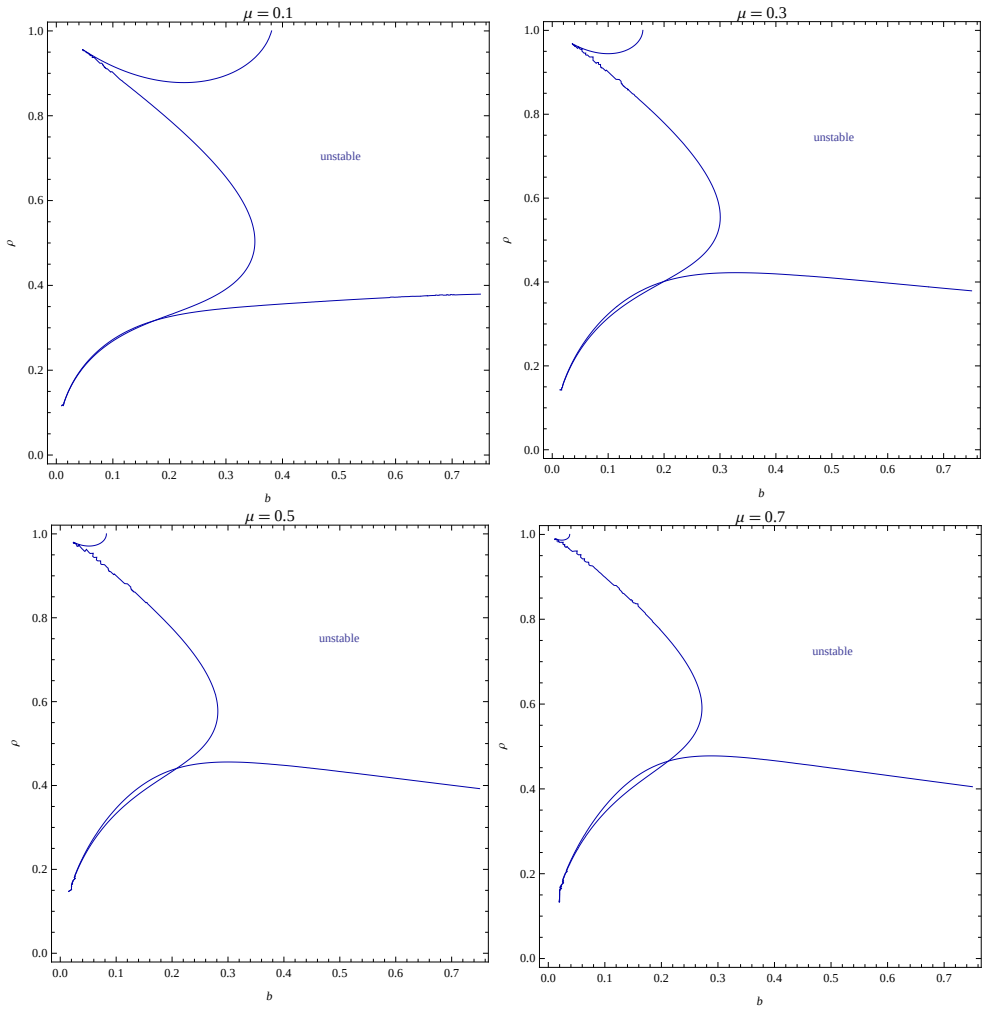

Figure 15: Linear instability regions for the zero-eccentricity equilibrium of counter-rotating centroids: The plane of b and ρ for different values of μ.

figure 15, the instability region is well defined in the plane. For large ρ (nearly equal semi-major axes), the instability region is wider in terms of the softening b. It gets narrower with decreasing ρ. The structure and the shape of the regions in the (b, ρ) plane do not change significantly with changing the mass ratio μ. Instead, they remain similar with a minor modification in the range of instability at large ρ.

B. Nonlinear Dynamics of Counter-rotating Centroids

As mentioned before, the full dynamics of counter-rotating centroids is governed by the four non-linear equations. There is no simple method to solve this system of equations due to its non-linearity. However, the underlying Hamiltonian, corresponding to a two-degree-of-freedom system, can tell us much about qualitatively different kinds of dynamical behavior of the system (equilibrium, stability, instability, etc...) through phase space analysis. To be able to plot the phase portrait in a two-dimensional plan, we convert our two-degree-of-freedom Hamiltonian system into a one-degree-of-freedom system by making use of a conserved quantity of the system. Let us now write the full centroid Hamiltonian in the following compact form:

$$\begin{aligned} H &= -\frac{\omega_+}{2}\left(u_+^2+v_+^2\right)-\frac{\omega_-}{2}\left(u_-^2+v_-^2\right)+\omega_c\left(u_+u_--v_+v_-\right) \\ &\quad -\eta_+\left(u_+^2+v_+^2\right)^2-\eta_-\left(u_-^2+v_-^2\right)^2 \\ &\quad -\frac{M}{\sqrt{a_+}}\gamma_c\left(u_+^2+v_+^2\right)\left(u_-^2+v_-^2\right)-\frac{M}{\sqrt{a_+}}\lambda_c\left(u_+u_--v_+v_-\right)^2 \\ &\quad +\left(\varepsilon_+\left(u_+^2+v_+^2\right)+\varepsilon_-\left(u_-^2+v_-^2\right)\right)\left(u_+u_--v_+v_-\right) \end{aligned}$$

where

$$
\begin{aligned}
\omega_+ &= 2\left(M_+\left(\alpha_{++}+\frac{\beta_{++}}{2}\right)+M_-\sqrt{\frac{a_-}{a_+}}\alpha_{cp}\right)\\
\omega_- &= 2\left(M_-\left(\alpha_{--}+\frac{\beta_{--}}{2}\right)+M_+\alpha_{cm}\right)\\
\omega_c &= \beta_c\sqrt{M_+M_-}\left(\frac{a_-}{a_+}\right)^{\frac{1}{4}}\\
\eta_+ &= M_-\frac{\sqrt{a_-}}{a_+\mu_+}\left(\chi_{cp}-\frac{\alpha_{cp}}{4}\right)\\
&\quad+\frac{M}{\sqrt{a_+}}\left(\chi_{++}-\frac{\alpha_{++}}{4}+\frac{\kappa_{++}}{4}+\frac{3\nu_{++}}{4}-\frac{\beta_{++}}{8}+\frac{\gamma_{++}+\lambda_{++}}{2}\right)\\
\eta_- &= M_+\frac{1}{\sqrt{a_-}\mu_-}\left(\chi_{cm}-\frac{\alpha_{cm}}{4}\right)\\
&\quad+\frac{M}{\sqrt{a_-}}\left(\chi_{--}-\frac{\alpha_{--}}{4}+\frac{\kappa_{--}}{4}+\frac{3\nu_{--}}{4}-\frac{\beta_{--}}{8}+\frac{\gamma_{--}+\lambda_{--}}{2}\right)\\
\varepsilon_+ &= Ma_+^{-\frac{3}{4}}a_-^{\frac{1}{4}}\sqrt{\frac{\mu_-}{\mu_+}}\left(\kappa_{cp}-\frac{\beta_c}{8}\right)\\
\varepsilon_- &= M\left(a_+a_-\right)^{-\frac{1}{4}}\sqrt{\frac{\mu_+}{\mu_-}}\left(\kappa_{cm}-\frac{\beta_c}{8}\right)
\end{aligned}
$$

We now perform the following change of variables $(u_+,v_+),(u_-,v_-)\to(\psi_+,L_+),(\psi_-,L_-)$ where

$$
\begin{aligned}
u_+ &= \sqrt{2L_+}\sin\psi_+ & \psi_+ &= \arctan\frac{u_+}{v_+}\\
v_+ &= \sqrt{2L_+}\cos\psi_+ & L_+ &= \frac{{u_+}^2+{v_+}^2}{2}\\
u_- &= \sqrt{2L_-}\sin\psi_- & \psi_- &= \arctan\frac{u_-}{v_-}\\
v_- &= \sqrt{2L_-}\cos\psi_- & L_- &= \frac{{u_-}^2+{v_-}^2}{2}
\end{aligned}
$$

Written in terms of $(e_+^{\mathrm{c}},g_+^{\mathrm{c}})$ and $(e_-^{\mathrm{c}},g_-^{\mathrm{c}})$, the new variables become

$$
\begin{aligned}
\psi_+ &= -g_+^c & \psi_- &= g_-^{\mathrm{c}}\\
L_+ &= \frac{1}{2}\mu_+\sqrt{a_+}{e_+^c}^2 & L_- &= \frac{1}{2}\mu_-\sqrt{a_-}{e_-^{\mathrm{c}}}^2
\end{aligned}
$$

Written in terms of the new variables ψ_+, L_+, ψ_- and L_-, the full centroid Hamiltonian becomes:

$$\begin{aligned} H &= -\omega_+ L_+ - \omega_- L_- - 2\omega_c \sqrt{L_+ L_-}\cos(\psi_+ + \psi_-) \\ &\quad -4\eta_+ L_+^2 - 4\eta_- L_-^2 - 4\frac{M}{\sqrt{a_+}}\gamma_c L_+ L_- \\ &\quad -4\frac{M}{\sqrt{a_+}}\lambda_c L_+ L_- \cos^2(\psi_+ + \psi_-) \\ &\quad -4\left(\varepsilon_+ L_+ + \varepsilon_- L_-\right)\sqrt{L_+ L_-}\cos(\psi_+ + \psi_-) \end{aligned}$$

We perform now a second change of variables $(\psi_+, L_+), (\psi_-, L_-) \rightarrow (\mathscr{V}, \mathscr{L}), (\Theta, \Sigma)$ where

$$\begin{aligned} \psi_+ &= \frac{\Theta + \mathscr{V}}{2} & \mathscr{V} &= \psi_+ - \psi_- \\ L_+ &= \Sigma + \mathscr{L} & \mathscr{L} &= \frac{L_+ - L_-}{2} \\ \psi_- &= \frac{\Theta - \mathscr{V}}{2} & \Theta &= \psi_+ + \psi_- \\ L_- &= \Sigma - \mathscr{L} & \Sigma &= \frac{L_+ + L_-}{2} \end{aligned}$$

Written in terms of (e_+^c, g_+^c) and (e_-^c, g_-^c), the new variables become

$$\begin{aligned} \mathscr{V} &= -(g_+^c + g_-^c) \\ \mathscr{L} &= \frac{\mu_+\sqrt{a_+}}{4} {e_+^c}^2 - \frac{\mu_-\sqrt{a_-}}{4} {e_-^c}^2 \\ \Theta &= g_-^c - g_+^c \\ \Sigma &= \frac{\mu_+\sqrt{a_+}}{4} {e_+^c}^2 + \frac{\mu_-\sqrt{a_-}}{4} {e_-^c}^2 \end{aligned}$$

Written in terms of the new variables $\mathscr{V}$, $\mathscr{L}$, Θ and Σ, the full centroid Hamiltonian becomes:

$$\begin{aligned} H &= -(\omega_+ + \omega_-)\Sigma - (\omega_+ - \omega_-)\mathscr{L} - 2\omega_c\sqrt{\Sigma^2 - \mathscr{L}^2}\cos\Theta \\ &\quad -4(\eta_+ + \eta_-)\Sigma^2 - 4(\eta_+ + \eta_-)\mathscr{L}^2 - 8(\eta_+ - \eta_-)\Sigma\mathscr{L} \\ &\quad -4\frac{M}{\sqrt{a_+}}\gamma_c(\Sigma^2 - \mathscr{L}^2) - 4\frac{M}{\sqrt{a_+}}\lambda_c(\Sigma^2 - \mathscr{L}^2)\cos^2\Theta \\ &\quad -4((\varepsilon_+ + \varepsilon_-)\Sigma + (\varepsilon_+ - \varepsilon_-)\mathscr{L})\sqrt{\Sigma^2 - \mathscr{L}^2}\cos\Theta \end{aligned}$$

Note that $\mathscr{V}$ is not present in the Hamiltonian and $\mathscr{L}$ is a constant of motion. Hence the Hamiltonian becomes function of only two variables Σ and Θ, where $\mathscr{L}$ is considered as a parameter. We transform now to the Cartesian-type canonical variables, $(\Theta, \Sigma) \to (U, V)$ where

$$\begin{aligned} U &= \sqrt{2(\Sigma - \mathscr{L})}\sin\Theta & \Theta &= \arctan\frac{U}{V} \\ V &= \sqrt{2(\Sigma - \mathscr{L})}\cos\Theta & \Sigma &= \frac{U^2 + V^2}{2} + \mathscr{L} \end{aligned}$$

In order to get sense of the new variables U and V, we relate them to (e_+^c, g_+^c) and (e_-^c, g_-^c), the eccentricity and the orientation of the centroids (fig 16).

$$\begin{aligned} U^2 + V^2 &= \mu_-\sqrt{a_-}{e_-^c}^2 \\ U/V &= \tan(g_-^c - g_+^c) \end{aligned}$$

with

$$\mu_+\sqrt{a_+}{e_+^c}^2 = 4\mathscr{L} + \mu_-\sqrt{a_-}{e_-^c}^2 = 4\mathscr{L} + U^2 + V^2$$

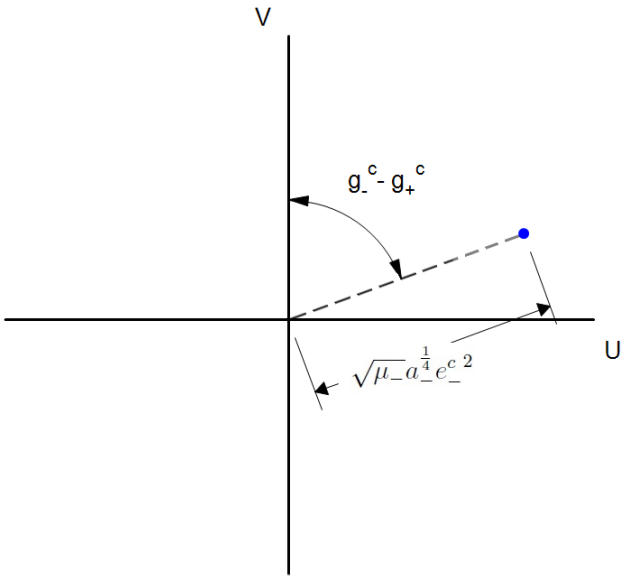

Figure 16: The meaning of e_-^c, g_+^c and g_-^c in the (U,V) phase space for counter-rotating centroids.

Written in terms of (U,V), the full one-degree-of-freedom centroid Hamiltonian becomes:

$$\begin{aligned} H &= -\frac{1}{2}(\omega_+ + \omega_-)\left(U^2+V^2\right) - \left(\eta_+ + \eta_- + \frac{M}{\sqrt{a_+}}\gamma_c\right)\left(U^2+V^2\right)^2 \\ &\quad -4\left(2\eta_+ + \frac{M}{\sqrt{a_+}}\gamma_c\right)\left(U^2+V^2\right)\mathscr{L} - \frac{1}{2}\omega_c V\sqrt{U^2+V^2+4\mathscr{L}} \\ &\quad -\frac{M}{\sqrt{a_+}}\lambda_c V^2\left(U^2+V^2+4\mathscr{L}\right) - 2\omega_+\mathscr{L} - 16\eta_+\mathscr{L}^2 \\ &\quad -\frac{1}{2}\left((\varepsilon_+ + \varepsilon_-)\left(U^2+V^2\right) + 4\varepsilon_+\mathscr{L}\right)V\sqrt{U^2+V^2+4\mathscr{L}} \end{aligned}$$

Since our system is now a one-degree-of-freedom system, plotting the isocontours of H is then enough for visualizing the phase portrait of the system. The parameters that control this phase portrait are $(\mathscr{L},\rho,\mu,b)$. Since H is independent of time, the centroid Hamiltonian of the system conserves itself. The centroid Hamiltonian also conserves the quantity $\mathscr{L}$ given in terms of e_+^c and e_-^c by:

$$\mathscr{L} = \frac{\mu_+\sqrt{a_+}}{4}e_+^{c\,2} - \frac{\mu_-\sqrt{a_-}}{4}e_-^{c\,2}$$

From the previous equation, we can see that $\mathscr{L}$ represents the difference between the mass-axis-weighted eccentricity of the prograde centroid and the mass-axis-weighted eccentricity of the retrograde centroid up to a scale of $\frac{1}{4}$. In other words, $\mathscr{L}$ represents the difference between the mass-axis-weighted average eccentricity of the prograde rings and the mass-axis-weighted average eccentricity of the retrograde rings up to $\frac{1}{4}$ (at the level of ring populations). Written in terms of u_+, v_+, u_- and v_-, $\mathscr{L}$ becomes

$$\mathscr{L} = \frac{u_+^2 + v_+^2}{4} - \frac{u_-^2 + v_-^2}{4}$$

Knowing that the total angular momentum of the counter-rotating stars is:

$$L_{\text{total}} = M_+\sqrt{GM_\bullet a_+} - M_-\sqrt{GM_\bullet a_-} - 2M\sqrt{GM_\bullet}\left(\frac{u_+^2 + v_+^2}{4} - \frac{u_-^2 + v_-^2}{4}\right)$$

one can also interpret $\mathscr{L}$ as the deficit in the total angular momentum of the counter-rotating stars due to orbital eccentricity, up to a scale of $(2M\sqrt{GM_\bullet})$. Since M_+, M_-, a_+ and a_- are all constant in time, the conservation of $\mathscr{L}$ implies the conservation of the total angular momentum L_{total} of the counter-rotating stars.

Hence, during the evolution of centroids, stars may exchange angular momentum with each other, but keeping the total angular momentum constant at its initial value. This angular momentum exchange is the reason of dynamical instability present in the system. Actually, a star may give or take angular momentum from another star in the same population. Moreover, for any increment (or decrement) in the angular momentum of the prograde population, there must be an increment (or decrement) in the angular momentum of the retrograde population such that the total angular momentum of the two populations stays constant.

In what follows, we explore the structure of nonlinear dynamics of counter-rotating centroids for the two cases of $\mathscr{L} = 0$ and $\mathscr{L} \neq 0$.

1. Nonlinear dynamics for $\mathscr{L} = 0$

$\mathscr{L} = 0$ means that the mass-axis-weighted eccentricity of the prograde centroid is equal to the mass-axis-weighted eccentricity of the retrograde centroid. It also means that the total angular momentum of the counter-rotating stars is at the value corresponding to circular (non-eccentric) orbits only (i.e. no excess or deficit due to orbital eccentricity). The $\mathscr{L} = 0$ case includes as a special case the zero-eccentricity where the prograde centroid eccentricity and the retrograde centroid eccentricity are both equal to zero. In order to explore the effect of the mass ratio μ on the dynamics of counter-rotating centroids, we follow the structure of the phase portrait as a function of μ at given values of ρ and b, when $\mathscr{L} = 0$.

Figure 17 shows the isocontours of H in the (U,V) phase space for different values of μ, when $\mathscr{L} = 0$, $\rho = 1$ and $b = 0.1$. In addition to the zero-eccentricity equilibrium P_2 discussed in the linearized dynamics, figure 17 shows two additional equilibria P_1 and P_3.

P_1 is always stable, it has $U = 0$ and $V < 0$ (i.e. $g_-^c - g_+^c = \pi$) which corresponds to uniformly precessing eccentric centroids with anti-aligned periapses. With increasing μ, P_1 remains stable and shifts continuously to lower values of V corresponding to higher eccentricity.

P_2 has $U = 0$ and $V = 0$, which corresponds to non-eccentric centroids. It remains stable till $\mu = 0.4435$ where it becomes unstable by merging with P_3 and remains unstable with further increase in μ. P_2 always remains at the same location $U = 0$ and $V = 0$.

P_3 is always unstable, it has $U = 0$ and $V > 0$ (i.e. $g_-^c - g_+^c = 0$) which corresponds to uniformly precessing eccentric centroids with aligned periapses. At μ around 0.3, P_3 starts shifting towards P_2 till it merges with P_2 at $U = 0$ and $V = 0$ as mentioned before.

In order to explore the effect of the semi-major-axis ratio ρ on the dynamics of counter-rotating centroids, we follow the structure of the phase portrait as a function of ρ at given values of μ and b, when $\mathscr{L} = 0$.

Figure 18 and 19 show the isocontours of H in the (U,V) phase space for different values of ρ, when $L = 0$, $\mu = 0.1$ and $b = 0.1$. As we have seen before, for $\mathscr{L} = 0$ and $\mu = 0.1$, the phase space contains three equilibrium points; a stable point P_1 at $U = 0$ and $V < 0$, a stable point P_2 at $U = 0$ and $V = 0$ and an unstable point P_3 at $U = 0$ and $V > 0$.

P_1: with decreasing ρ, P_1 remains stable and shifts continuously to lower values of V corresponding to higher eccentricity, until it approaches $\rho = 0.96$ where it disappears and leaves the phase space with only two equilibria, P_2 and P_3.

P_2: with decreasing ρ, P_2 remains stable till $\rho = 0.9169$ where it becomes unstable by merging with P_3. P_2 remains unstable till $\rho = 0.8988$ where it becomes stable again and remains stable afterwards. P_2 doesn't change location but remains at $U = 0$ and $V = 0$ for all ρ.

P_3: with decreasing ρ, P_3 remains unstable and shifts continuously to lower eccentricity towards P_2. At $\rho = 0.9169$ P_3 merges with P_2 at $U = 0$ and $V = 0$ and remains merged till $\rho = 0.8988$ where it emerges from P_2. During the merging and emerging of P_3 and P_2, P_3 converts from positive to negative values of V corresponding to uniformly precessing eccentric centroids switching from aligned to anti-aligned periapses. With further decrease of ρ, P_3 shifts continuously to lower values of V, corresponding to higher eccentricity till it disappears around 0.55 and leaves the phase space with only one equilibrium point P_2.

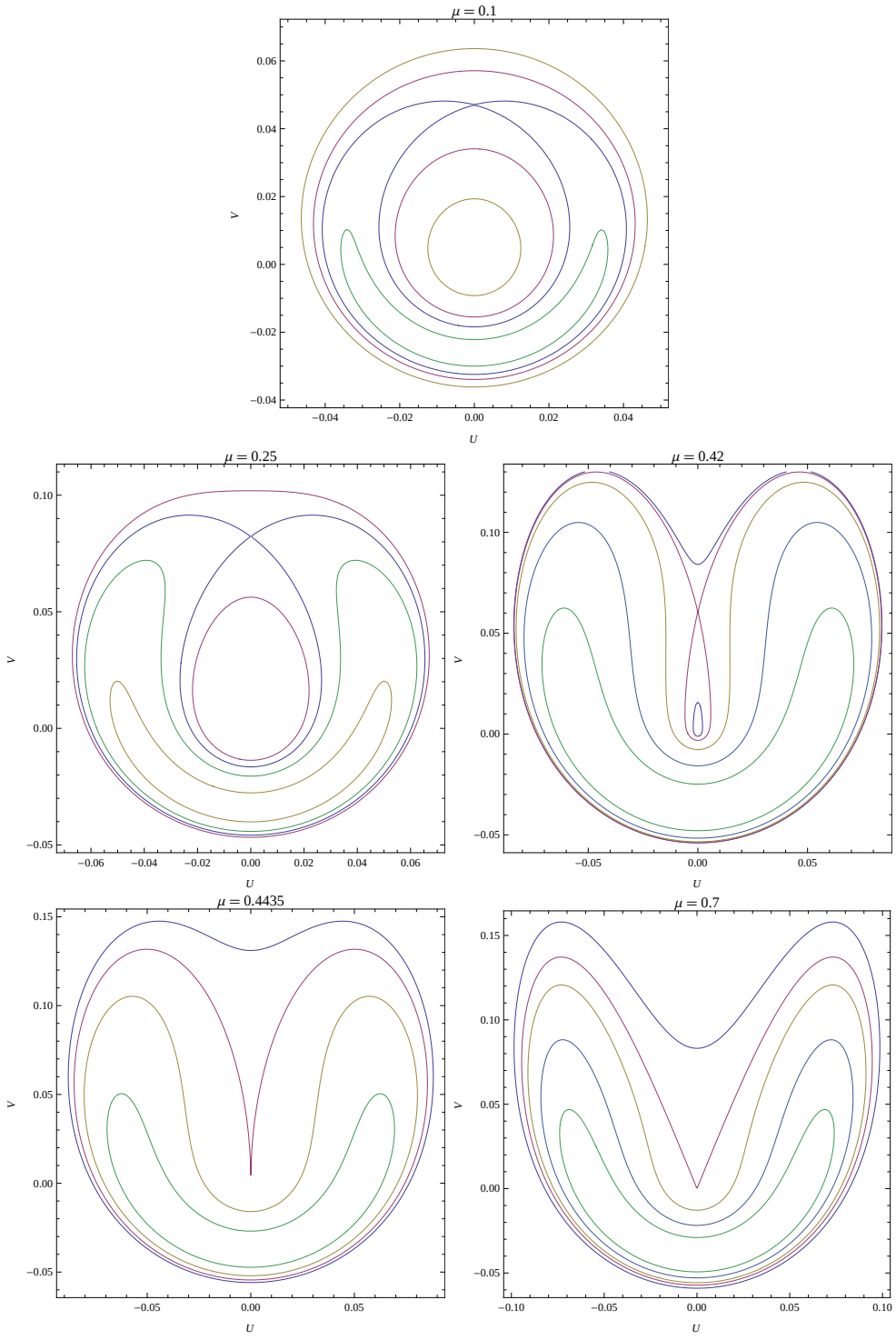

Figure 17: Phase portraits of counter-rotating centroids for different values of μ, $\mathscr{L} = 0$, $\rho = 1$ and $b = 0.1$.

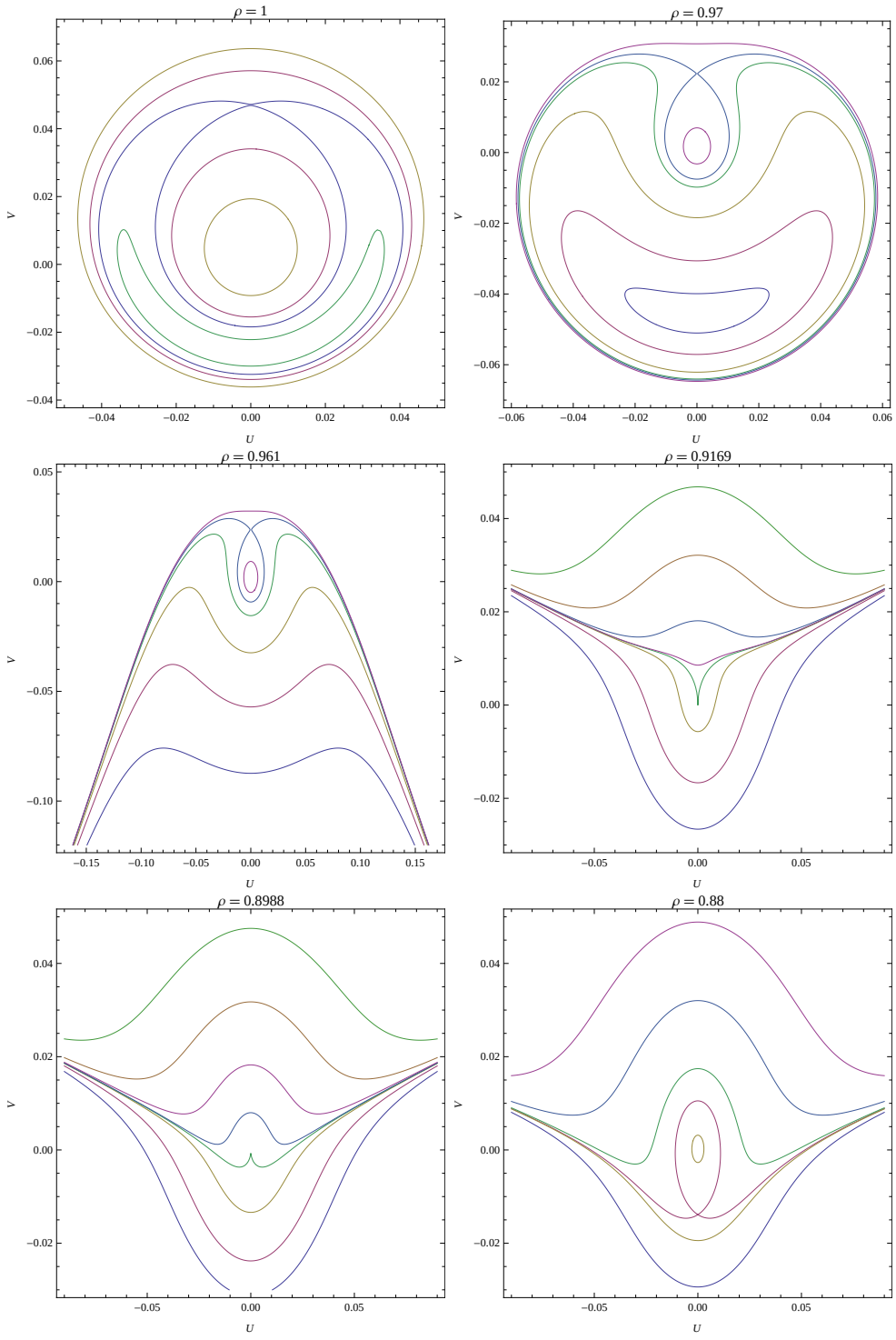

Figure 18: Phase portraits of counter-rotating centroids for different values of ρ, $\mathscr{L} = 0$, $\mu = 0.1$ and $b = 0.1$. (Part 1)

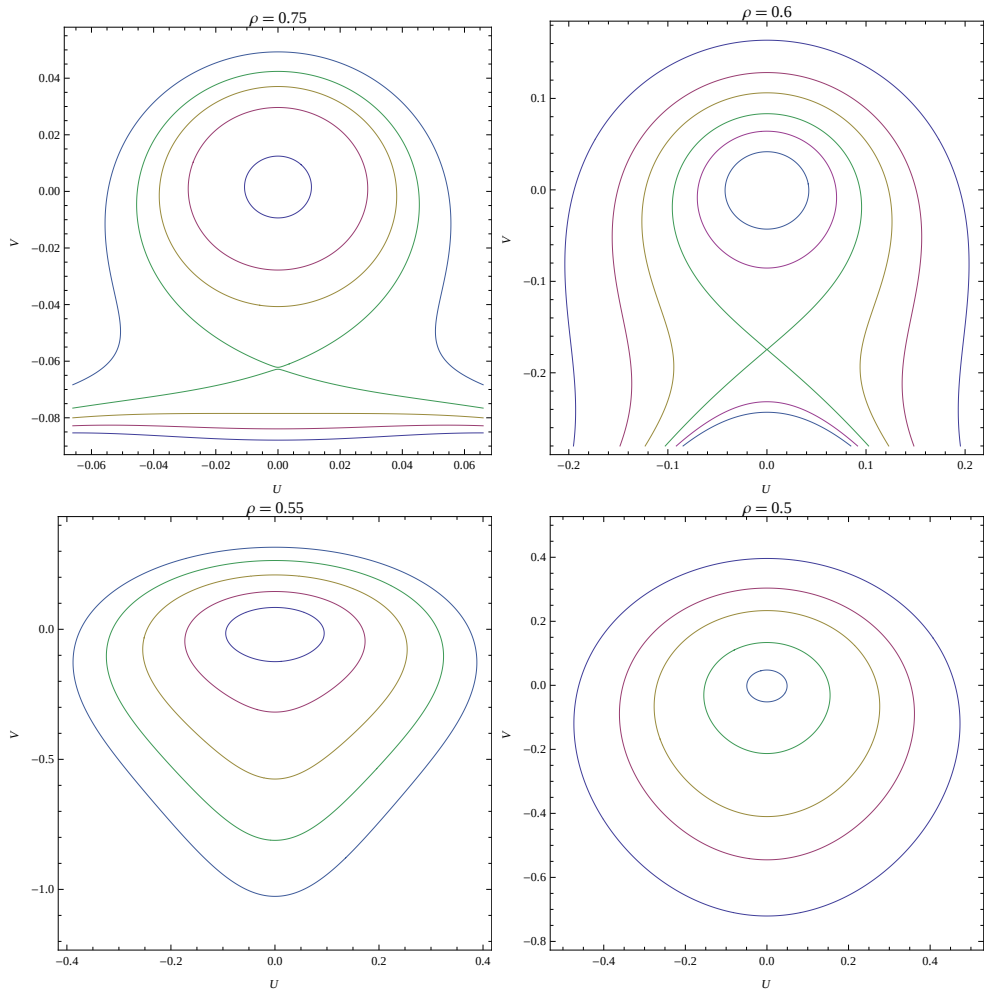

Figure 19: Phase portraits of counter-rotating centroids for different values of ρ, $\mathscr{L} = 0$, $\mu = 0.1$ and $b = 0.1$. (Part 2)

2. *Nonlinear dynamics for* $\mathscr{L} \neq 0$

$\mathscr{L} \neq 0$ means that the prograde and the retrograde centroids have different mass-axis-weighted eccentricity. It also means that there is an excess or deficit in the total angular momentum of the counter-rotating stars due to orbital eccentricity.

In order to explore the effect of $\mathscr{L}$ on the dynamics of counter-rotating centroids, we follow the structure of the phase portrait as a function of $\mathscr{L}$ at given values of μ and b, when $\rho = 1$.

Figure 20 shows the isocontours of H in the (U,V) phase space for different values of $\mathscr{L}$, when $\rho = 1$, $\mu = 0.1$ and $b = 0.1$. As we have seen, for $\mathscr{L} = 0$ and $\mu = 0.1$, the phase space contains three equilibrium points; a stable point P_1 at $U = 0$ and $V < 0$, a stable point P_2 at $U = 0$ and $V = 0$ and an unstable point P_3 at $U = 0$ and $V > 0$.

P_1: with increasing $\mathscr{L}$, P_1 remains stable and shifts continuously to higher values of V till it converts from negative to positive V at $\mathscr{L} = 0.0031$. This conversion corresponds to uniformly precessing eccentric centroids switching from anti-aligned to aligned periapses. With further increase in $\mathscr{L}$, P_1 remains stable until $\mathscr{L} = 0.0434$ where it becomes unstable and gives presence to two off-axis stable equilibria corresponding to non-aligned uniformly precessing eccentric centroids. With further increase in $\mathscr{L}$, P_1 shifts continuously to higher values of V corresponding to higher eccentricity.

P_2: with increasing $\mathscr{L}$, P_2 remains stable and shifts continuously to higher values of V corresponding to higher eccentricity till it hits $\mathscr{L} = 0.0272$ where it disappears by merging with P_3.

P_3: with increasing $\mathscr{L}$, P_3 remains unstable and shifts continuously to higher values of V corresponding to higher eccentricity till it hits $\mathscr{L} = 0.0272$ where it disappears by merging with P_2 as mentioned before.

In order to explore the effect of the semi-major-axis ratio ρ on the dynamics of counter-rotating eccentric centroids, we follow the structure of the phase portrait as a function of ρ at given values of μ and b, when $\mathscr{L} = 0.1$.

Figure 21 and 22 show the isocontours of H in the (U,V) phase space for different values of ρ, when $\mathscr{L} = 0.1$, $\mu = 0.1$ and $b = 0.1$. As seen before, for $\mathscr{L} = 0.1$ and $\rho = 1$, the phase space of the counter-rotating centroids contains three equilibrium points; two off-axis stable points P_4 and P_5 at $U \neq 0$ and $V > 0$ and one unstable point P_2 at $U = 0$ and $V > 0$.

With decreasing ρ, P_4 and P_5 remain stable and shift to lower eccentricity towards P_2, until $\rho = 0.99996$ where they merge with P_2 and transform it to a stable point at $U = 0$ and $V > 0$ corresponding to uniformly precessing eccentric centroids with aligned periapses.

With further decrease in ρ, P_2 remains stable and shifts to lower eccentricity till $\rho = 0.962$ where it arrives at $U = 0$ and $V = 0$ and remains there afterwards.

With further decrease in ρ, an unstable point takes place at $U = 0$ and $V < 0$ and starts shifting towards P_2 till $\rho = 0.952$ where it merges with P_2 and make the stable equilibrium at $U = 0$ and $V = 0$ disappear leaving the phase space with no equilibrium points.

Afterwards, the phase space remains without equilibria till $\rho = 0.8$ where two new equilibrium points emerge at $U = 0$ and $V < 0$. The first equilibrium P_6 always remains stable and shifts continuously to higher values of V, till it arrives at $U = 0$ and $V = 0$ and remains their afterwards. The second equilibrium P_7 remains unstable and shifts continuously to lower values of V, till $\rho = 0.5$ where a new stable equilibrium P_8 takes place at $U = 0$ and $V_8 < V_7$

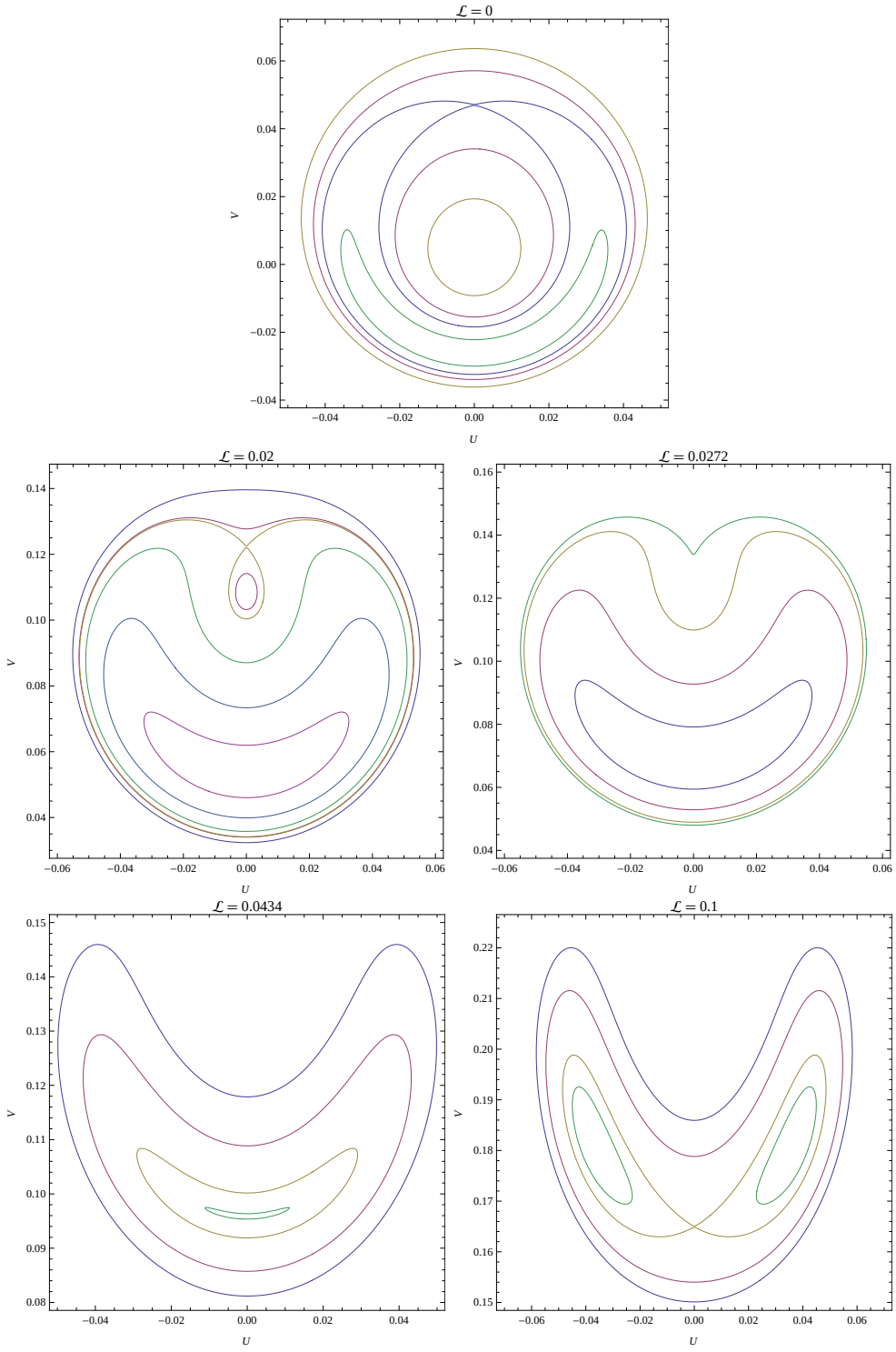

Figure 20: Phase portraits of counter-rotating centroids for different values of $\mathscr{L}$, $\rho = 1$, $\mu = 0.1$ and $b = 0.1$.

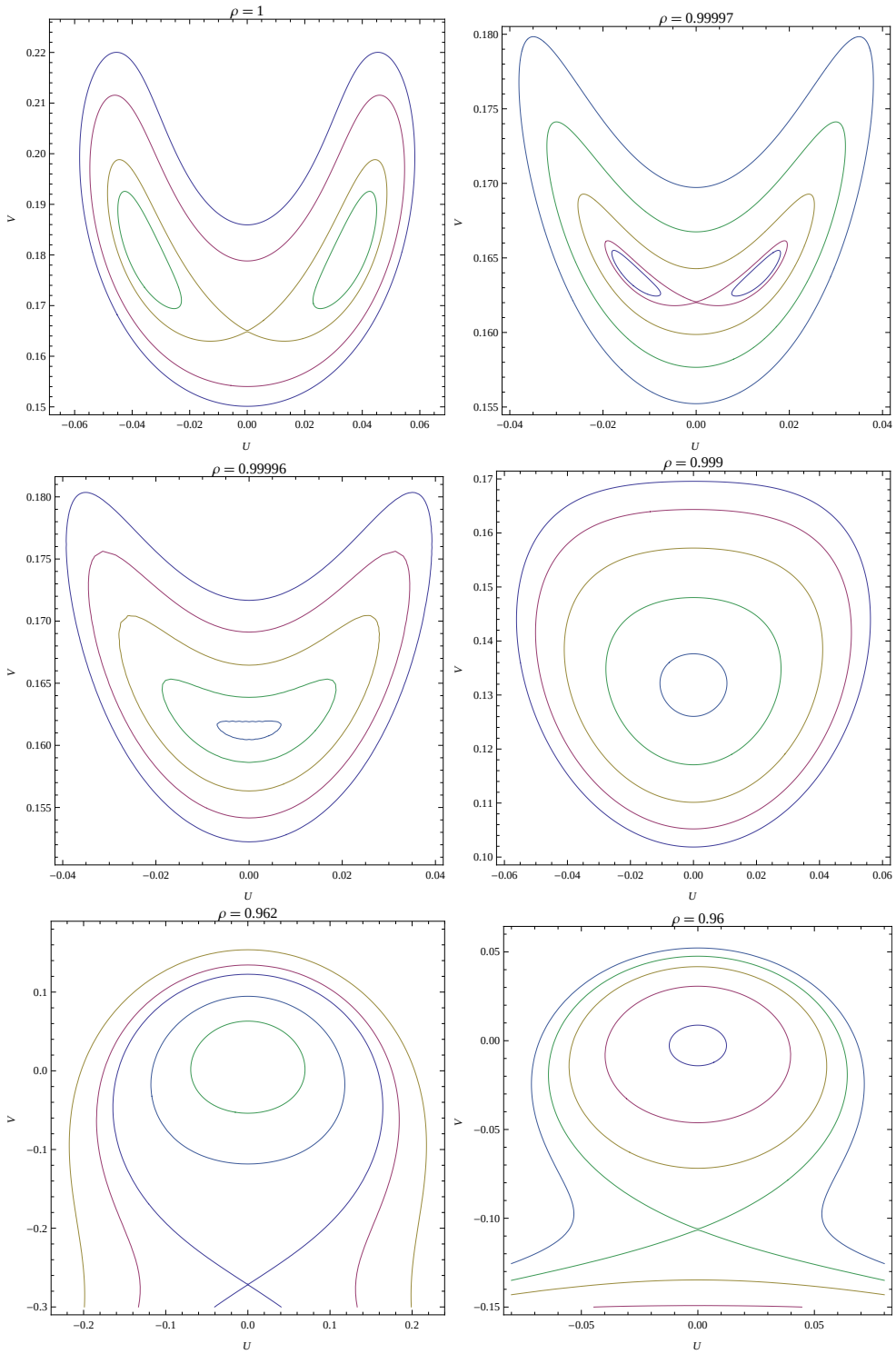

Figure 21: Phase portraits of counter-rotating centroids for different values of ρ, $\mathscr{L} = 0.1$, $\mu = 0.1$ and $b = 0.1$. (Part 1)

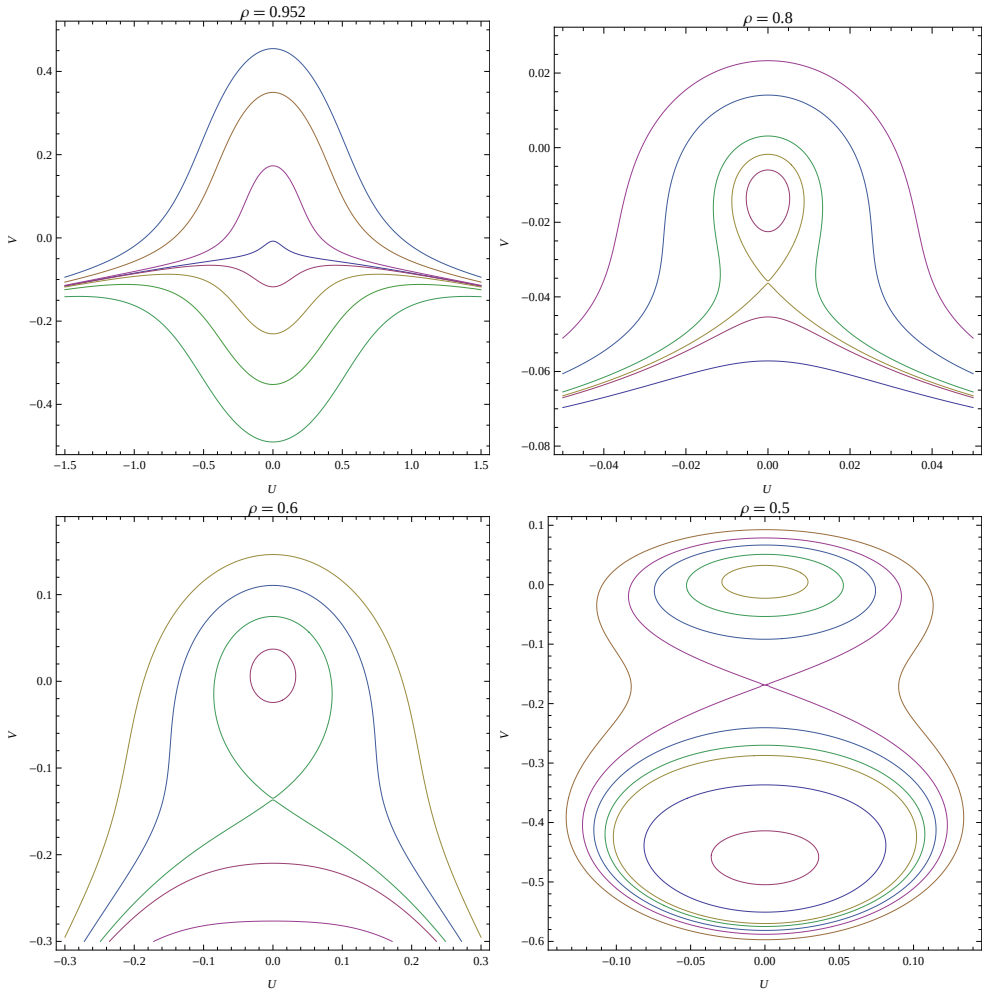

Figure 22: Phase portraits of counter-rotating centroids for different values of ρ, $\mathscr{L} = 0.1$, $\mu = 0.1$ and $b = 0.1$. (Part 2)

C. Nonlinear Dynamics of co-rotating centroids

To appreciate the effects of counter rotation and the corresponding phase space which is full of bifurcations, we explore the contrast case of co-rotating centroids. The corresponding full (nonlinear) Hamiltonian is given by

$$
\begin{aligned}
H \;=\; & -\left(M_+\left(\alpha_{++}+\frac{\beta_{++}}{2}\right)+M_-\sqrt{\frac{a_-}{a_+}}\alpha_{cp}\right)\left(u_+^2+v_+^2\right) \\
& -\left(M_-\left(\alpha_{--}+\frac{\beta_{--}}{2}\right)+M_+\alpha_{cm}\right)\left(u_-^2+v_-^2\right) \\
& -\beta_c\sqrt{M_+M_-}\left(\frac{a_-}{a_+}\right)^{\frac{1}{4}}\left(u_+u_-+v_+v_-\right) \\
& -\left(M_-\frac{\sqrt{a_-}}{a_+\mu_+}\left(\chi_{cp}-\frac{\alpha_{cp}}{4}\right)\right. \\
& \left.+\frac{M}{\sqrt{a_+}}\left(\chi_{++}-\frac{\alpha_{++}}{4}+\frac{\kappa_{++}}{4}+\frac{3\nu_{++}}{4}-\frac{\beta_{++}}{8}+\frac{\gamma_{++}+\lambda_{++}}{2}\right)\right)\left(u_+^2+v_+^2\right)^2 \\
& -\left(M_+\frac{1}{\sqrt{a_-}\mu_-}\left(\chi_{cm}-\frac{\alpha_{cm}}{4}\right)\right. \\
& \left.+\frac{M}{\sqrt{a_-}}\left(\chi_{--}-\frac{\alpha_{--}}{4}+\frac{\kappa_{--}}{4}+\frac{3\nu_{--}}{4}-\frac{\beta_{--}}{8}+\frac{\gamma_{--}+\lambda_{--}}{2}\right)\right)\left(u_-^2+v_-^2\right)^2 \\
& -\frac{M}{\sqrt{a_+}}\gamma_c\left(u_+^2+v_+^2\right)\left(u_-^2+v_-^2\right)-\frac{M}{\sqrt{a_+}}\lambda_c\left(u_+u_-+v_+v_-\right)^2 \\
& -\left(Ma_+^{-\frac{3}{4}}a_-^{\frac{1}{4}}\sqrt{\frac{\mu_-}{\mu_+}}\left(\kappa_{cp}-\frac{\beta_c}{8}\right)\left(u_+^2+v_+^2\right)\right. \\
& \left.+M\left(a_+a_-\right)^{-\frac{1}{4}}\sqrt{\frac{\mu_+}{\mu_-}}\left(\kappa_{cm}-\frac{\beta_c}{8}\right)\left(u_-^2+v_-^2\right)\right)\left(u_+u_-+v_+v_-\right)
\end{aligned}
$$

where the $+$ and $-$ sub-indices both refer to prograde populations with different semi-major axes a_+ and a_-, respectively. As mentioned before, the centroid Hamiltonian can tell us much about qualitatively different kinds of dynamical behavior of the system (equilibrium, stability, instability, etc...) through phase space analysis. To be able to plot the phase portrait in a two-dimensional plan, we convert our two-degree-of-freedom Hamiltonian system into a one-degree-of-freedom system by making use of a conserved quantity of the system. Let us now write the full centroid Hamiltonian in the following compact

form:

$$\begin{aligned} H &= -\frac{\omega_+}{2}\left(u_+^2+v_+^2\right)-\frac{\omega_-}{2}\left(u_-^2+v_-^2\right)+\omega_c\left(u_+u_--v_+v_-\right) \\ &\quad -\eta_+\left(u_+^2+v_+^2\right)^2-\eta_-\left(u_-^2+v_-^2\right)^2 \\ &\quad -\frac{M}{\sqrt{a_+}}\gamma_c\left(u_+^2+v_+^2\right)\left(u_-^2+v_-^2\right)-\frac{M}{\sqrt{a_+}}\lambda_c\left(u_+u_--v_+v_-\right)^2 \\ &\quad +\left(\varepsilon_+\left(u_+^2+v_+^2\right)+\varepsilon_-\left(u_-^2+v_-^2\right)\right)\left(u_+u_--v_+v_-\right) \end{aligned}$$

where

$$\begin{aligned} \omega_+ &= 2\left(M_+\left(\alpha_{++}+\frac{\beta_{++}}{2}\right)+M_-\sqrt{\frac{a_-}{a_+}}\alpha_{cp}\right) \\ \omega_- &= 2\left(M_-\left(\alpha_{--}+\frac{\beta_{--}}{2}\right)+M_+\alpha_{cm}\right) \\ \omega_c &= \beta_c\sqrt{M_+M_-}\left(\frac{a_-}{a_+}\right)^{\frac{1}{4}} \\ \eta_+ &= M_-\frac{\sqrt{a_-}}{a_+\mu_+}\left(\chi_{cp}-\frac{\alpha_{cp}}{4}\right) \\ &\quad +\frac{M}{\sqrt{a_+}}\left(\chi_{++}-\frac{\alpha_{++}}{4}+\frac{\kappa_{++}}{4}+\frac{3\nu_{++}}{4}-\frac{\beta_{++}}{8}+\frac{\gamma_{++}+\lambda_{++}}{2}\right) \\ \eta_- &= M_+\frac{1}{\sqrt{a_-}\mu_-}\left(\chi_{cm}-\frac{\alpha_{cm}}{4}\right) \\ &\quad +\frac{M}{\sqrt{a_-}}\left(\chi_{--}-\frac{\alpha_{--}}{4}+\frac{\kappa_{--}}{4}+\frac{3\nu_{--}}{4}-\frac{\beta_{--}}{8}+\frac{\gamma_{--}+\lambda_{--}}{2}\right) \\ \varepsilon_+ &= Ma_+^{-\frac{3}{4}}a_-^{\frac{1}{4}}\sqrt{\frac{\mu_-}{\mu_+}}\left(\kappa_{cp}-\frac{\beta_c}{8}\right) \\ \varepsilon_- &= M\left(a_+a_-\right)^{-\frac{1}{4}}\sqrt{\frac{\mu_+}{\mu_-}}\left(\kappa_{cm}-\frac{\beta_c}{8}\right) \end{aligned}$$

We now perform the following change of variables $(u_+, v_+), (u_-, v_-) \rightarrow (\psi_+, L_+), (\psi_-, L_-)$ where

$$
\begin{aligned}
u_+ &= \sqrt{2L_+}\sin\psi_+ & \psi_+ &= \arctan\frac{u_+}{v_+} \\
v_+ &= \sqrt{2L_+}\cos\psi_+ & L_+ &= \frac{{u_+}^2 + {v_+}^2}{2} \\
u_- &= \sqrt{2L_-}\sin\psi_- & \psi_- &= \arctan\frac{u_-}{v_-} \\
v_- &= \sqrt{2L_-}\cos\psi_- & L_- &= \frac{{u_-}^2 + {v_-}^2}{2}
\end{aligned}
$$

Written in terms of $(e^{\mathrm{c}}_+, g^{\mathrm{c}}_+)$ and $(e^{\mathrm{c}}_-, g^{\mathrm{c}}_-)$, the new variables are

$$
\begin{aligned}
\psi_+ &= -g^c_+ & \psi_- &= g^{\mathrm{c}}_- \\
L_+ &= \frac{1}{2}\mu_+\sqrt{a_+}{e^c_+}^2 & L_- &= \frac{1}{2}\mu_-\sqrt{a_-}{e^{\mathrm{c}}_-}^2
\end{aligned}
$$

Written in terms of the new variables ψ_+, L_+, ψ_- and L_-, the full centroid Hamiltonian becomes:

$$
\begin{aligned}
H \;=\; & -\omega_+ L_+ - \omega_- L_- + 2\omega_c\sqrt{L_+L_-}\cos(\psi_+ - \psi_-) \\
& -4\eta_+ L_+^2 - 4\eta_- L_-^2 - 4\frac{M}{\sqrt{a_+}}\gamma_c L_+ L_- \\
& -4\frac{M}{\sqrt{a_+}}\lambda_c L_+ L_- \cos^2(\psi_+ - \psi_-) \\
& +4\left(\varepsilon_+ L_+ + \varepsilon_- L_-\right)\sqrt{L_+L_-}\cos(\psi_+ - \psi_-)
\end{aligned}
$$

We perform now a second change of variables $(\psi_+, L_+), (\psi_-, L_-) \rightarrow (\mathscr{V}, \Sigma), (\Theta, \mathscr{L})$ where

$$\begin{aligned} \psi_+ &= \frac{\Theta + \mathscr{V}}{2} & \mathscr{V} &= \psi_+ - \psi_- \\ L_+ &= \mathscr{L} + \Sigma & \Sigma &= \frac{L_+ - L_-}{2} \\ \psi_- &= \frac{\Theta - \mathscr{V}}{2} & \Theta &= \psi_+ + \psi_- \\ L_- &= \mathscr{L} - \Sigma & \mathscr{L} &= \frac{L_+ + L_-}{2} \end{aligned}$$

Written in terms of (e_+^c, g_+^c) and (e_-^c, g_-^c), the new variables are

$$\begin{aligned} \mathscr{V} &= -(g_+^c + g_-^c) \\ \Sigma &= \frac{\mu_+\sqrt{a_+}}{4} {e_+^c}^2 - \frac{\mu_-\sqrt{a_-}}{4} {e_-^c}^2 \\ \Theta &= g_-^c - g_+^c \\ \mathscr{L} &= \frac{\mu_+\sqrt{a_+}}{4} {e_+^c}^2 + \frac{\mu_-\sqrt{a_-}}{4} {e_-^c}^2 \end{aligned}$$

Written in terms of the new variables $\mathscr{V}$, Σ, Θ and $\mathscr{L}$, the full centroid Hamiltonian becomes:

$$\begin{aligned} H &= -(\omega_+ + \omega_-)\mathscr{L} - (\omega_+ - \omega_-)\Sigma + 2\omega_c\sqrt{\mathscr{L}^2 - \Sigma^2}\cos\mathscr{V} \\ &\quad -4(\eta_+ + \eta_-)\mathscr{L}^2 - 4(\eta_+ + \eta_-)\Sigma^2 - 8(\eta_+ - \eta_-)\mathscr{L}\Sigma \\ &\quad -4\frac{M}{\sqrt{a_+}}\gamma_c(\mathscr{L}^2 - \Sigma^2) - 4\frac{M}{\sqrt{a_+}}\lambda_c(\mathscr{L}^2 - \Sigma^2)\cos^2\mathscr{V} \\ &\quad +4((\varepsilon_+ + \varepsilon_-)\mathscr{L} + (\varepsilon_+ - \varepsilon_-)\Sigma)\sqrt{\mathscr{L}^2 - \Sigma^2}\cos\mathscr{V} \end{aligned}$$

Note that Θ is not present in the Hamiltonian and $\mathscr{L}$ is a constant of motion. Hence the Hamiltonian becomes function of only two variables $\mathscr{V}$ and Σ, where $\mathscr{L}$ is considered as a parameter. We transform now to the Cartesian-type canonical variables, $(\mathscr{V}, \Sigma) \rightarrow (U, V)$

where

$$U = \sqrt{2(\mathscr{L}-\Sigma)}\cos\mathscr{V} \qquad \mathscr{V} = \arctan\frac{V}{U}$$
$$V = \sqrt{2(\mathscr{L}-\Sigma)}\sin\mathscr{V} \qquad \Sigma = \mathscr{L} - \frac{U^2+V^2}{2}$$

In order to get sense of the new variables U and V, we relate them to (e_+^c, g_+^c) and (e_-^c, g_-^c), the eccentricity and the orientation of the centroids. (Fig. 23)

$$\begin{aligned} U^2+V^2 &= \mu_-\sqrt{a_-}e_-^{c\,2} \\ V/U &= \tan(-(g_+^c+g_-^c)) \end{aligned}$$

with

$$\mu_+\sqrt{a_+}e_+^{c\,2} = 4\mathscr{L} - \mu_-\sqrt{a_-}e_-^{c\,2} = 4\mathscr{L} - \left(U^2+V^2\right)$$

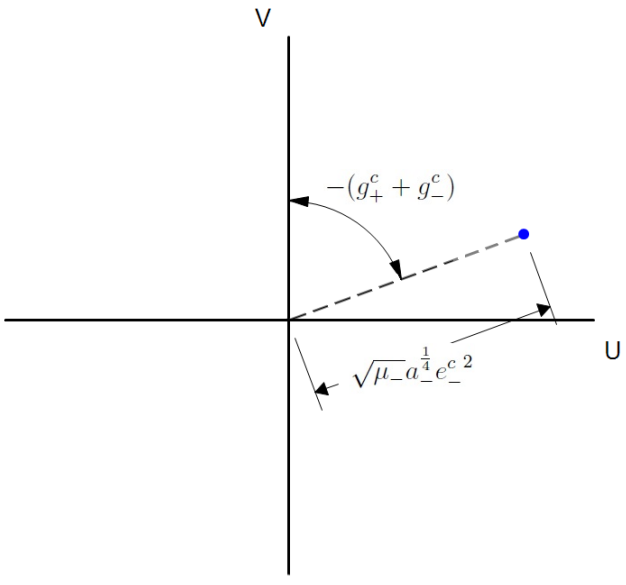

Figure 23: The meaning of e_-^c, g_+^c and g_-^c in the (U,V) phase space for co-rotating centroids.

Written in terms of (U,V), the full one-degree-of-freedom centroid Hamiltonian

becomes:

$$\begin{aligned} H &= \frac{1}{2}(\omega_+ - \omega_-)\left(U^2+V^2\right) - \left(\eta_+ + \eta_- - \frac{M}{\sqrt{a_+}}\gamma_c\right)\left(U^2+V^2\right)^2 \\ &\quad -4\left(\frac{M}{\sqrt{a_+}}\gamma_c - 2\eta_+\right)\left(U^2+V^2\right)\mathscr{L} + \omega_c U\sqrt{4\mathscr{L} - (U^2+V^2)} \\ &\quad -\frac{M}{\sqrt{a_+}}\lambda_c U^2\left(4\mathscr{L} - \left(U^2+V^2\right)\right) - 2\omega_+\mathscr{L} - 16\eta_+\mathscr{L}^2 \\ &\quad +\left(4\varepsilon_+\mathscr{L} - (\varepsilon_+ - \varepsilon_-)\left(U^2+V^2\right)\right)U\sqrt{4\mathscr{L} - (U^2+V^2)} \end{aligned}$$

In order to visualize the phase portrait of the co-rotating centroids, we plot the isocontours of H in the (U,V) plane. Since H is independent of time, the centroid Hamiltonian of the system conserves itself. The centroid Hamiltonian also conserves the quantity $\mathscr{L}$ given in terms of e_+^c and e_-^c by:

$$\mathscr{L} = \frac{\mu_+\sqrt{a_+}}{4}{e_+^c}^2 + \frac{\mu_-\sqrt{a_-}}{4}{e_-^c}^2$$

From the previous equation, we can see that $\mathscr{L}$ represents the sum of the mass-axis-weighted eccentricity of the two centroids up to a scale of $\frac{1}{4}$.
Written in terms of u_+, v_+, u_- and v_-, $\mathscr{L}$ becomes

$$\mathscr{L} = \frac{u_+^2+v_+^2}{4} + \frac{u_-^2+v_-^2}{4}$$

Knowing that the total angular momentum of the prograde-prograde system of stars is:

$$L_{\text{total}} = M_+\sqrt{GM_\bullet a_+} + M_-\sqrt{GM_\bullet a_-} - 2M\sqrt{GM_\bullet}\left(\frac{u_+^2+v_+^2}{4} + \frac{u_-^2+v_-^2}{4}\right)$$

one can also interpret $\mathscr{L}$ as the deficit in the total angular momentum of all the stars due to orbital eccentricity, up to a scale of $(2M\sqrt{GM_\bullet})$. Since M_+, M_-, a_+ and a_- are all constant in time, the conservation of $\mathscr{L}$ implies the conservation of the total angular momentum L_{total} of the stars.

Hence, during the evolution of centroids, stars may exchange angular momentum with each other, but keeping the total angular momentum constant at its initial value. A star may give or take angular momentum from another star in any population. Moreover, for any increment (or decrement) in the angular momentum of the first population, there must be a decrement (or increment) in the angular momentum of the second population and vise versa, such that the total angular momentum of the two populations stays constant.

For $\mathscr{L} = 0$, the eccentricity of the first and the second centroids should both be equal to zero. In this case, the phase portrait of the co-rotating centroids reduces to one point at $U = 0$ and $V = 0$ (zero-eccentricity point).

For $\mathscr{L} \neq 0$, the phase portrait is much richer than the zero case, however it is still bounded to certain region depending on $\mathscr{L}$. In this case, the eccentricity of the centroids cannot exceed certain values depending on the value of $\mathscr{L}$. In what follows, we explore the structure of nonlinear dynamics of co-rotating centroids for $\mathscr{L} = 1$.

$\mathscr{L} = 1$ means that the mass-axis-weighted eccentricity of the first centroid and the mass-axis-weighted eccentricity of the second centroid should add up to one. It also means that there is a deficit of $2M\sqrt{GM_\bullet}$ in the total angular momentum of the co-rotating stars due to orbital eccentricity.

Figure 24 shows the isocontours of H in the (U,V) phase space when $\mathscr{L} = 1$, $\rho = 1$, $\mu = 0.1$ and $b = 0.1$.

The phase space shown in figure 24, contains six equilibrium points:

P_1 is stable , it has $U < 0$ and $V = 0$ (i.e. $g^c_+ + g^c_- = -\pi$) which corresponds to uniformly precessing eccentric co-rotating centroids with non-aligned periapses in general.

P_2 is stable, it has $U > 0$ and $V < 0$.

P_3 is stable, it has $U > 0$ and $V > 0$.

$U > 0$ and $V \lesseqgtr 0$ corresponds to uniformly precessing eccentric co-rotating centroids with nonaligned periapses in general.

P_4 and P_5 are both unstable with $U > 0$ and $V = 0$.

P_6 is stable, it has $U > 0$ and $V = 0$.

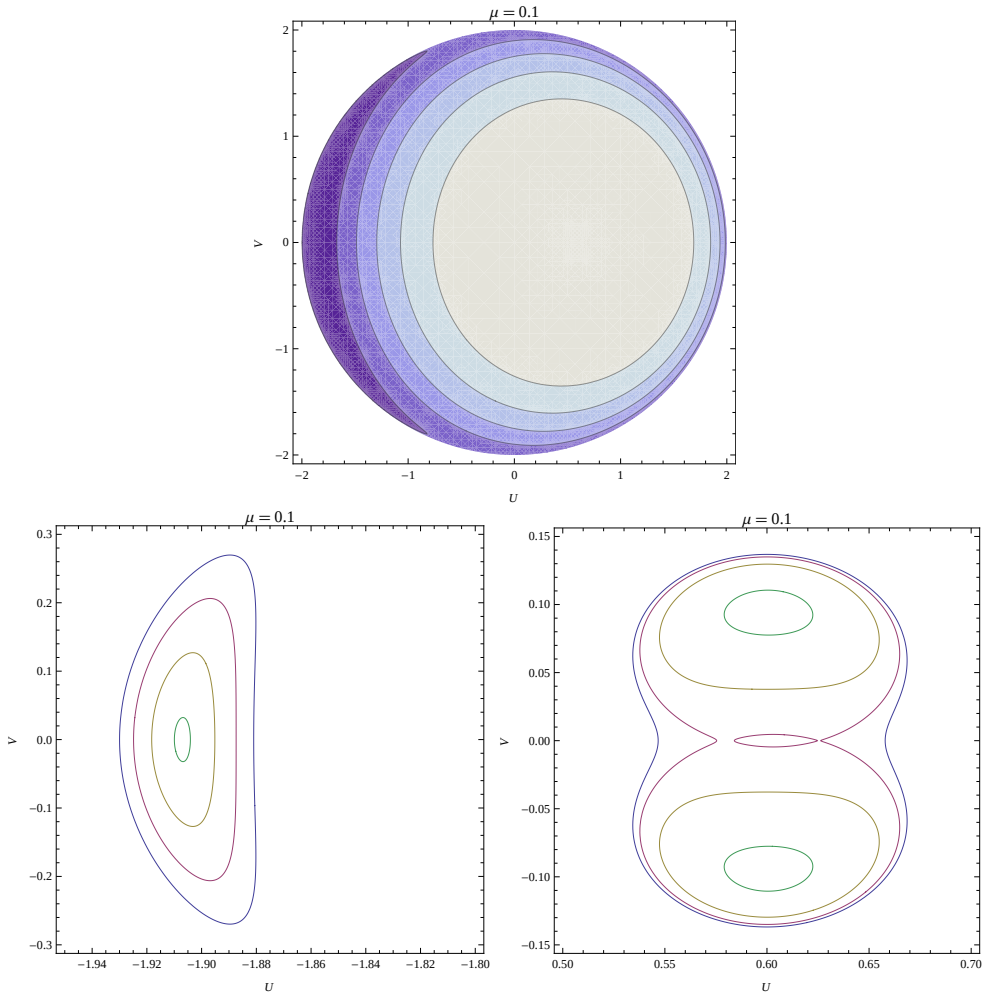

Figure 24: Phase portraits of co-rotating centroids for $\mu = 0.1$, when $\mathscr{L} = 1$, $\rho = 1$ and $b = 0.1$.

$U > 0$ and $V = 0$ implies $g_+^c + g_-^c = 0$ which corresponds to uniformly precessing eccentric co-rotating centroids with symmetric periapses about the reference axis.

To see the effect of the mass ratio μ on the structure of the phase space, we plot the phase portrait of the system for two additional values of μ.

Figure 25 and Figure 26 show the isocontours of H in the (U,V) phase space for two different values of μ, $\mu = 0.25$ and $\mu = 0.7$, when $\mathscr{L} = 1$, $\rho = 1$ and $b = 0.1$.

The structure of the phase space of the co-rotating centroids doesn't change with changing μ. There is no any bifurcation in this case. For instance, with increasing μ, P_1 remains stable and shifts continuously to lower eccentricity. P_2 and P_3 also remain stable and shift continuously away from the U axis to higher eccentricity. P_4, P_5 and P_6, all shift to higher

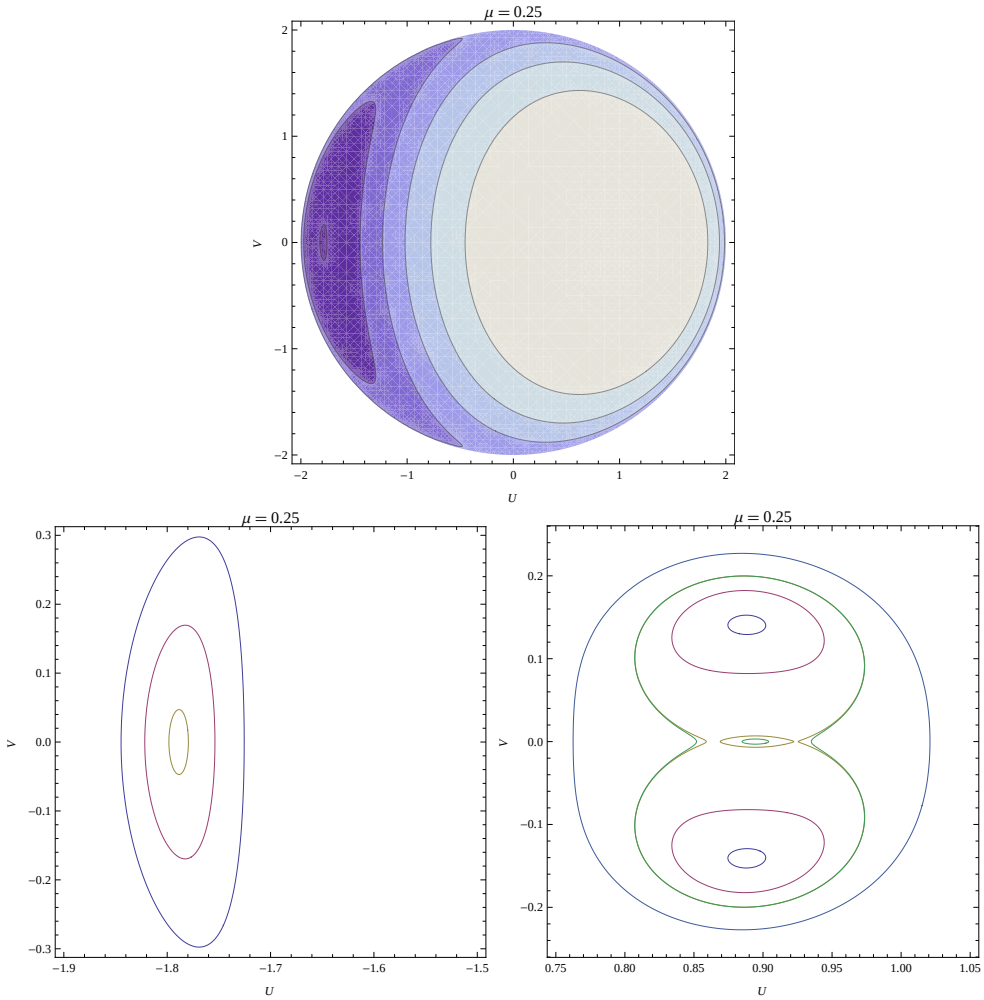

Figure 25: Phase portraits of co-rotating centroids for $\mu = 0.25$, when $\mathscr{L} = 1$, $\rho = 1$ and $b = 0.1$.

eccentricity without changing nature (stable or unstable).

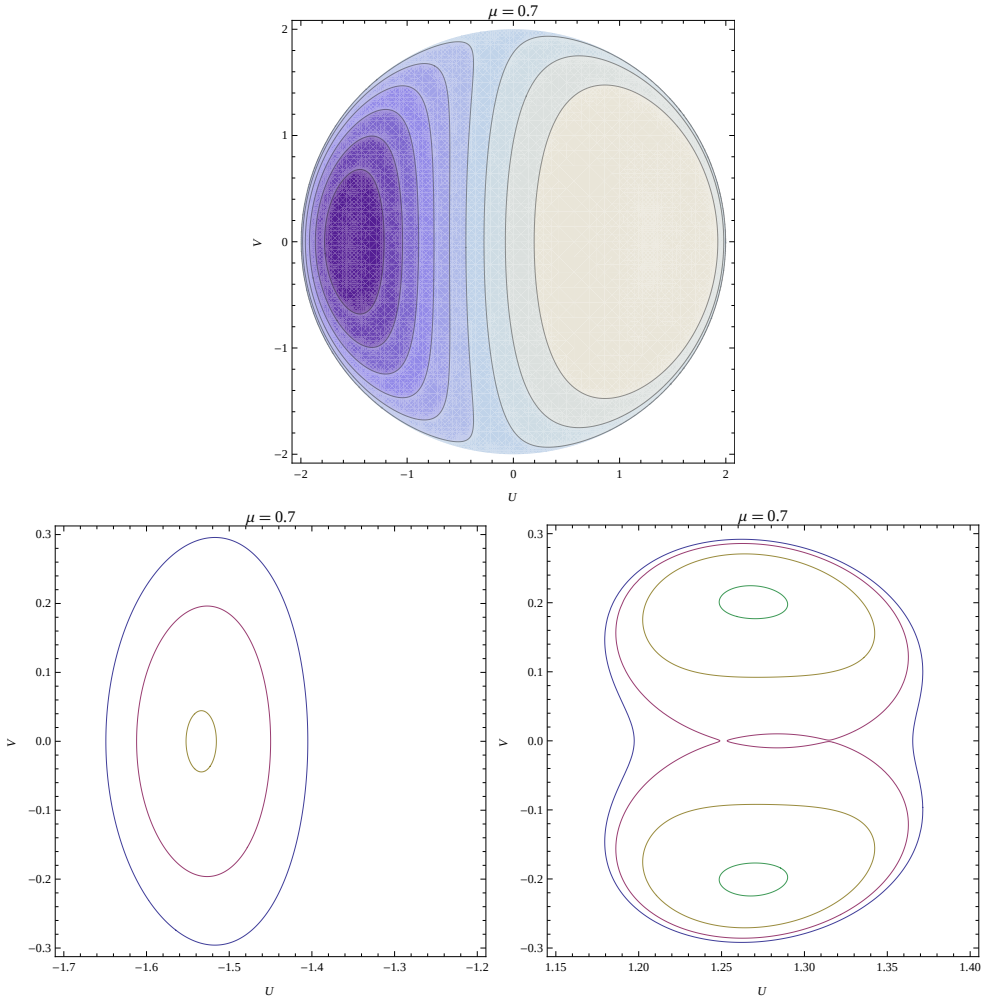

Figure 26: Phase portraits of co-rotating centroids for $\mu = 0.7$, when $\mathscr{L} = 1$, $\rho = 1$ and $b = 0.1$.

CHAPTER V

SUMMARY AND CONCLUSIONS

In this report, we formulated the self-consistent problem of a collisionless cluster of stars around a massive black hole. The stars were assumed to move on nearly Keplerian orbits around the black hole due to the dominance of the black hole within its radius of influence. As we were not interested in the fast orbital phase, we averaged over it and we focused our work on the study of the secular evolution of the resulting massive rings. In addition, the orbit averaging results in the conservation of the semi-major axis of each ring and leads to a four dimensional phase space instead of six. For instance, we were left with the four Delaunay variables describing individual rings: (1) the magnitude of the angular momentum, (2) the z-projection of the angular momentum, (3) the argument of the periapsis and (4) the argument of the ascending node. Allowing for counter rotation between stars, we divided our rings into two populations, prograde and retrograde. Having the self-consistency and the absence of collisions in the problem, we represented the two populations of rings by two separate distribution functions (DFs), prograde and retrograde, which satisfy two separate collionsless Boltzmann equations (CBEs) governing the slow dynamics of the system. The two distribution functions depend self-consistently on two separate Hamiltonians (ring Hamiltonians), the orbit-averaged gravitational potential energy between the stars. On the other hand, each ring Hamiltonian depends on the two distribution functions since the two populations of rings are gravitationally coupled together. Restricting our problem to populations of rings of small eccentricities, we then expanded the ring Hamiltonians to fourth order in the eccentricities (with coefficients that depend on both the prograde and the retrograde DFs). The Hamiltonian expansion was taken from a previous work by Touma and Sridhar [11]. We transformed then to new canonical variables suitable to such restriction. Using Jeans' theorem, we constructed

then our time-dependent DFs by taking them to be some physically allowed functions of an approximate invariant of the Hamiltonians. The resulting DFs turned out to be such that their isocontours are ellipses centered at moving origins. Those moving origins, referred to as the centroids, satisfy four equations. In the limit where the dispersion in the eccentricities were smaller than the centroid eccentricities, the slow dynamics of the counter-rotating disks was well described by the independent dynamics of the two centroids with no necessity for studying the shape dynamics of the DFs. The four centroid equations are four autonomous first order nonlinear ODEs. They constituted an integrable system. For instance, we showed that these four equations can be derived from an underlying Hamiltonian corresponding to a two-degree-of-freedom system. This system turned out to be integrable due to the presence of two conserved quantities, the Hamiltonina itself, and another quantity corresponding to the total angular momentum of the two populations. The work done to this point is a generalization of a previous work by Touma and Sridhar [11]. Here, we assigned different semi-major axes for different populations where the retrograde population were assumed to have the smaller one.

Studying the centroid dynamics linearly was a straightforward task by solving the linearized four centroid equations. However in the nonlinear case, the centroid Hamiltonian constituted a helpful way to explore the dynamics of the system where solving the four nonlinear centroid equations were an uneasy task.

We started by studying the linear dynamics of the system where we identified an equilibrium point at the origin corresponding to two populations of circular orbits. We studied then the linear stability of this zero-eccentricity equilibrium based on the three parameters controlling the linear dynamics (the semi-major axis ratio ρ, the mass ratio μ and the softening b). In fact, we followed the instability region of the zero-eccentricity equilibrium in the (b, μ) plane for different semi-major axis ratio. For a given semi-major axis ratio and softening, there were critical values of the mass ratio where the zero-eccentricity equilibrium was unstable. This instability corresponds to uniformly precessing disks of growing or damped eccentricities whereas the stability of the system corresponds to uniformly

precessing disks of fixed centroid eccentricities. In order to explore the effect of ρ in a more accurate way, we followed the instability region of the zero-eccentricity equilibrium in the (b,ρ) plane for different values of μ. The plane was divided into two well defined regions corresponding to the stability and the instability. In general, the instability region was wider for large ρ corresponding to nearly equal semi-major axes and got narrower with decreasing ρ. Hence, we concluded that the instability of the zero-eccentricity equilibrium is more probable for large values of ρ.

We moved next to the nonlinear dynamics. In order to be able to plot the phase portrait of the system in a two dimensional plane, we reduced the dynamics to a one-degree-of-freedom system by making use of some canonical transformations and the conservation of the total angular momentum. The results of the nonlinear study can be summarized as follows:

We started with $\mathscr{L} = 0$ corresponding to stellar disks of total angular momentum equal to that of stars with circular orbits. First, we followed the phase space structure of zero-$\mathscr{L}$ disks as a function of their mass ratio, when their semi-major axes were equal and their softening was relatively small ($b = 0.1$). We noticed that, in addition to the zero-eccentricity equilibrium shown in the linear dynamics, the nonlinear dynamics of the system contains two additional equilibria. The first corresponds to uniformly precessing eccentric disks with anti-aligned periapses and remains stable for any mass ratio. The second corresponds to uniformly precessing eccentric disks with aligned periapses and remains unstable for all mass ratios.

We second followed the phase space structure of zero-$\mathscr{L}$ disks as a function of their semi-major axis ratio, when $\mu = 0.1$ and $b = 0.1$. Same as before, the phase space initially (at $\rho = 1$) contained three equilibrium points. The first corresponds to uniformly precessing eccentric disks with anti-aligned periapses. It remains stable for all ρ below 0.961 and disappears afterwards. The second corresponds to non-eccentric disks. It remains stable till $\rho = 0.9169$ where it becomes unstable and stays until $\rho = 0.8988$. At $\rho = 0.8988$ it becomes stable again and remains stable afterwards. The third corresponds to uniformly

precessing eccentric disks with aligned periapses. It remains unstable for all values of ρ. However, it converts from aligned to anti-aligned periapses at $\rho = 0.8988$ and shifts to higher eccentricities till it disappears around $\rho = 0.55$.

For $\mathscr{L} \neq 0$ the dynamics of the system was so different. First, we followed the phase space structure as a function of $\mathscr{L}$, when their semi-major axes were equal, their mass ratio was 0.1 and their softening was relatively small ($b = 0.1$). The phase space initially (at $\mathscr{L} = 0$) contained three equilibrium points. The first corresponds to uniformly precessing eccentric disks with anti-aligned periapses. It starts initially stable and shifts continuously to lower eccentricities till it switches from anti-aligned to aligned periapses at $\mathscr{L} = 0.0031$. It remains stable until $\mathscr{L} = 0.0434$ where it becomes unstable and gives presence to two off-axis stable equilibria corresponding to non-aligned uniformly precessing eccentric centroids. The second corresponds to non-eccentric disks. It remains stable and shifts continuously to higher eccentricity till it hits $\mathscr{L} = 0.0272$ and disappears. The third corresponds to uniformly precessing eccentric disks with aligned periapses. It remains unstable and shifts continuously to higher eccentricity till it hits $\mathscr{L} = 0.0272$ and disappears.

We second followed the phase space structure of nonzero-$\mathscr{L}$ disks as a function of their semi-major axis ratio, when $\mathscr{L} = 0.1$, $\mu = 0.1$ and $b = 0.1$. The phase space initially (at $\rho = 1$) contained three equilibrium points; two off-axis stable points and one unstable point. With decreasing ρ, the two off-axis stable points disappear by merging with the third unstable point into a stable point corresponding to uniformly precessing eccentric disks with aligned periapses. The new stable point remains stable till $\rho = 0.962$ where it merges with a new-born unstable point and both disappear. Afterwards, the phase space remains without equilibria till $\rho = 0.8$ where two new equilibrium points emerge. The first corresponds to uniformly precessing eccentric disks with aligned periapses and remains stable afterwards. The second corresponds to uniformly precessing eccentric disks with anti-aligned periapses and remains unstable afterwards. At $\rho = 0.5$ a new stable equilibrium takes place corresponding to uniformly precessing disks with anti-aligned

periapses.

A possible generalization is to allow for a range of different semi-major axes in each population of stars. In this case, the problem of two centroids becomes a multicentroid problem and provide an independent confirmation to the results found in the simpler problem, the presence of various uniformly precessing eccentric discs of different properties and nature which depend on several parameters like the angular momentum, the semi-major axis ratio and the mass ratio. Another generalization is to study the dynamics of three-dimensional cluster instead of planar cluster, where a third degree of freedom (inclination) would be added. In this case, the ring Hamiltonian would be expanded in terms of the inclination in addition to the eccentricity and the orientation. Although this would results in a little bit more complication at the level of inerrability, the three-dimensional generalization may provide a confirmation of the current results. Finally, as a third possible generalization, we could allow for different physically allowed DFs other than the delta functions at the centroids and study their shape dynamics in a direct way. These generalizations provide a larger framework to study the problem of stellar cluster around a black hole and lead to new features and properties of the dynamics.

BIBLIOGRAPHY

[1] N. Cretton, P.T. De Zeeuw, R.P. Van Der Marel, and H.W. Rix. Axisymmetric three-integral models for galaxies. *The Astrophysical Journal Supplement Series*, 124(2):383, 2008.

[2] S. Tremaine. Secular stability and instability in stellar systems surrounding massive objects. *The Astrophysical Journal*, 625(1):143, 2008.

[3] S. Tremaine. An eccentric disk model for the nucleus of m31. *arXiv preprint astro-ph/9502065*, 1995.

[4] M.V. Kazandjian and J.R. Touma. The doubling of stellar black hole nuclei. *arXiv preprint arXiv:1207.1108*, 2012.

[5] R. Bender, J. Kormendy, G. Bower, R. Green, J. Thomas, A.C. Danks, T. Gull, JB Hutchings, CL Joseph, ME Kaiser, et al. Hst stis spectroscopy of the triple nucleus of m31: two nested disks in keplerian rotation around a supermassive black hole. *The Astrophysical Journal*, 631(1):280, 2008.

[6] A.E. Roy. *Orbital motion*. Taylor & Francis, 2004.

[7] P. Hut, J. Makino, P. Teuben, and HP Bischof. Moving stars around. *The Art of Computational Science*, 2007.

[8] J. Binney and S. Tremaine. *Galactic dynamics*. Princeton university press, 1988.

[9] S Sridhar and J Touma. Stellar dynamics around black holes in galactic nuclei. *Monthly Notices of the Royal Astronomical Society*, 303(3):483–494, 1999.

[10] H. Goldstein, C.P. Poole, and J. Safko. *Classical mechanics*. 1980.

[11] J.R. Touma and S. Sridhar. Counter-rotating stellar discs around a massive black hole: self-consistent, time-dependent dynamics. *Monthly Notices of the Royal Astronomical Society*, 2012.

[12] V.I. Arnol'd. *Mathematical methods of classical mechanics*, volume 60. Springer, 1989.

[13] E Athanassoula, E Fady, JC Lambert, and A Bosma. Optimal softening for force calculations in collisionless n-body simulations. *Monthly Notices of the Royal Astronomical Society*, 314(3):475–488, 2000.